Measurement 235 (2024) 114949

Contents lists available at ScienceDirect

Measurement

journal homepage: www.elsevier.com/locate/measurement

Nondestructive global corrosion measurement using guided wavefield data

Beata Zima *, Emil Roch

Faculty of Mechanical Engineering and Ship Technology, Gdańsk University of Technology, 80-233 Gdańsk, Poland

ARTICLE INFO

Keywords:
Guided waves
Irregular plate
Corrosion degradation
Experimental tests
Innovative systems

ABSTRACT

Metallic structures often face degradation, and corrosion ranks among the most prevalent forms of deterioration. Accurate quantification of corrosion is crucial, especially for structures exposed to harsh environmental conditions, such as marine vessels and offshore installations. Because the traditional measurement methods based on scanning by ultrasonic gauge are time-consuming and provide only rough information on the thickness variability, there is a need to develop new robust and accurate diagnostics methods. This paper aims to investigate the corrosion monitoring of metal plates using guided wave propagation. Guided waves propagate within the entire volume of the specimen. If it is undamaged and isotropic, the velocity in all directions is the same, and the spreading wavefront takes a circular shape. The primary assumption presented in this paper is that the potential damage caused by corrosion leads to disturbance of this symmetry. The study shows Bilateral and Rotational Corrosion Symmetry Degree (BCSD and RCSD) functions, demonstrating a consistent decrease in symmetry values with increasing degree of degradation (DoD) caused by the corrosion process. The main aim of the study was to test the possibility of corrosion monitoring by using variable number of sensors comprising the transducer network. Also, the influence of the distance between the sensors affecting the size of the monitored area on the corrosion monitoring procedure was investigated. The paper contains the results of numerical and experimental campaigns conducted for corroded plates characterized by variable DoD and monitored using nine different transducers configurations. It is the first step in developing a novel measurement procedure specially designed for the ship and offshore industry. Therefore, because of the initial stage of the study, the last part of the paper discusses the limitations and drawbacks of the presented wave symmetry-based approach.

1. Introduction

Metallic structures often face degradation, and corrosion ranks among the most prevalent forms of deterioration [1–3]. Accurate quantification of corrosion is crucial, especially for structures exposed to harsh environmental conditions, such as marine vessels and offshore installations. The conventional nondestructive method, relying on ultrasonic testing endorsed by Classification Societies [4], has notable limitations. This method involves using a coupling agent, which may impact the structure's integrity [56], and is inherently time-intensive due to extensive surface preparation. Despite providing thickness maps, ultrasonic measurements are limited by the density and distribution of measurement points, making them less effective for localized damages like pitting corrosion.

For this reason, developing novel diagnostics methods that would allow for more effective and accurate thickness reduction estimation due to corrosion degradation is crucial for the industry. Guided wave propagation, particularly Lamb waves, offers a promising solution. Lamb waves can travel long distances without significant amplitude reduction, making them valuable for assessing thickness reduction and detecting localized pits and cracks [7]. The great potential of guided waves in diagnostics of various damage types like cracks [8,9], pits [10,11] or debondings [12,13] has been demonstrated in many papers. Because the guided waves are dispersive, their velocity is influenced by the specimen's thickness, forming the basis for wave-based diagnostic methods for general corrosion assessment. The main assumption of these methods is that the corrosion causes the thickness reduction which affects wave propagation velocity and the shape of the dispersion curves. Researchers have utilized dispersion curves [14], continuous wavelet transform, wave velocity measurement [15] to quantify corrosion damage. Various algorithms, such as those based on Riesz transform [16], time–frequency damage indices [11], nonlinear wave propagation [17] and coda interferometry [18] have been proposed for corrosion inspection. Despite these efforts, environmental conditions and

* Corresponding author.
E-mail address: beata.zima@pg.edu.pl (B. Zima).

https://doi.org/10.1016/j.measurement.2024.114949
Received 14 January 2024; Received in revised form 11 April 2024; Accepted 19 May 2024
Available online 23 May 2024

imperfect transducer attachment make complete defect characterization still very challenging. Moreover, guided waves present significant challenges in inverse problems. Even minor variations in input data can lead to substantial disparities in estimated thickness variability. Acquiring reference data from intact structures can enhance precision but is often impractical due to the associated costs. Therefore, there is a need for a novel, nondestructive technique that doesn't rely on reference data.

This paper considers different approach based on guided wave propagation in specimens subjected to general corrosion. This introduces an innovative method for assessing general corrosion levels by estimating the symmetry level of the propagating wavefront. Unlike previous studies [19], which explored symmetry breaking in signal patterns, our approach focuses on the circular shape of the wavefront influenced by thickness variations induced by general corrosion. Experimental tests, complemented by numerical analyses on plates with irregular surfaces, demonstrate the method's effectiveness. Notably, the proposed method requires less exact mode identification and is less sensitive to systematic errors in time of flight determination.

The main idea is based on assessing the propagating wavefront spreading in the tested structure. In the undamaged structure, we expect to observe a circular wavefront as the wave propagates with the same velocity in each direction. Due to corrosion degradation and irregular thickness reduction, one can expect the disturbance of the perfect circular wavefront shape. The ship and offshore industry have raised the need for a novel approach for plate-structure assessment. As mentioned, the traditional method which often incorporates standard ultrasonic measurements is very time-consuming and do not provide detailed information about the thickness variability of the, for example, ship hull. The presented method assumes that the limited number of measured signals may be used to assess the quality of the area surrounded by the sensors network. The concept is shown in Fig. 1. Instead of the information about the thickness in 8 selected points, we can measure the vibration caused by the propagation of guided wave, estimate the roughness of the entire area, and increase the possibility to detect the localized pits simultaneously.

The presented study is thus the introduction for developing the novel procedure and (from a further perspective) the device specially designed for ship diagnostics, reducing the measurement time and allowing for a more detailed assessment of the geometric variability of the tested structure. The developed device will be comprised of transducers mounted on the circle, which facilitate the assessment of the circular shape of the wavefront. However, the wavefront shape reconstruction accuracy strongly depends on the number of sensors in the network. The greater the number, the more information about the structure and the more detailed wavefront reconstruction. On the other hand, we want to avoid the possible difficulties with sensors mounting increasing proportionally to the network extent.

Moreover, the greater number of signals requires more extensive data processing. The next parameter crucial for the proper design of the device is its size and range of the monitored area. In the case of the significant distance between transducers, we can monitor the significant area during a single measurement. On the other hand, the information about the corrosion degradation level determined based on the symmetry assessment will only be rough. The greater the area monitored during the single measurement, the faster the measurement campaign is. However, increasing area is associated with decreasing resolution of the damage detection. All these aspects must be considered before the measurement system/device is designed for industry applications.

Within this study, the corrosion degradation assessment algorithm using the transducers' circular array will be tested for a variable number of sensors and the distance between them. The main aim is to test what is the influence of the transducers network extent and the distance between sensors on the corrosion degradation assessment. This study is the first step towards the initial design of the new diagnostics system for which certain initial parameters should be adopted, i.e. the number of sensors and the monitoring area. Supplementary to experimental tests, numerical analyses were conducted on plates featuring irregular surfaces modelled using random fields. The simulations covered plates with diverse characteristics, including varying average thickness (DoD), standard deviation of thickness variability, and the number of transducers within the network. Additionally, tests were conducted at different excitation frequencies to assess the sensitivity of distinct wavelengths to surface irregularities resulting from corrosion degradation. This study is the continuation of the research presented in [20].

The paper is organized as follows: Section 2 contains the background of the theoretical description of wave propagation in irregular plates, Section 3 contains a description of the material and methods. In Sections 4 and 5, numerical and experimental results are presented. Finally, Section 6 contains the main discussion, conclusions, and perspectives for future work.

2. Guided wave propagation in corrosion assessment

2.1. Wave propagation is specimens with variable thickness

The influence of variable thickness on wave propagation phenomena has been widely investigated in previous studies ([21–27]). Due to the dispersive nature of guided waves, their propagation velocity and the number of possible wave modes depend on material parameters, excitation frequency, and plate thickness. The relationships between frequency and velocity are described by dispersion equations which are formulated for the uniform geometry i.e., constant plate thickness. The reformulation of dispersion equations for prediction the average wave propagation velocity in specimens with variable thickness has been demonstrated in [22]. Let's consider the plate with non-uniform thickness (Fig. 2). To the aim of velocity assessment alongside the propagation path, the plate has been divided into N equal divisions with a length Δl with varying thickness, one can formulate the time needed to travel the distance Δl:

$$\Delta t_i = \frac{\Delta l_i}{c_{g_i}} \tag{1}$$

where c_{g_i} is the group velocity determined for the corresponding thickness d_i based on the explicitly given Lamb dispersion equations. If we

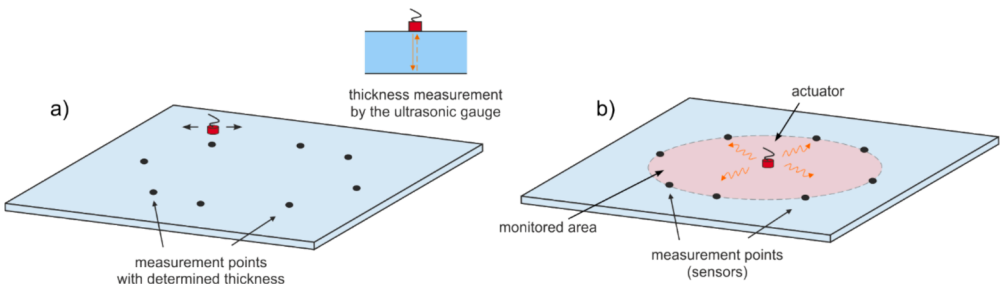

Fig. 1. Corrosion level assessment a) by the use of standard ultrasonic gauge and b) by the circular array of the sensor network.

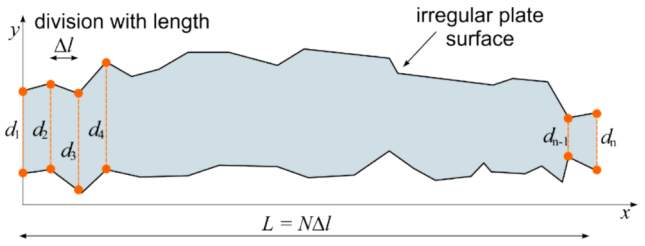

Fig. 2. Plate with variable geometry.

sum up the particular times of flight along with the distances Δl, we can derive the relationship for the total ToF along the distance L is a:

$$ToF = \sum_{i=1}^{N} t_i = \sum_{i=1}^{N} \frac{\Delta l}{c_{g_i}} = \Delta l \sum_{i=1}^{N} \frac{1}{c_{g_i}} \tag{2}$$

Therefore, the average velocity alongside the distance L is described as:

$$c_{g,mean} = \frac{L}{ToF} = \frac{L}{\Delta l \sum_{i=1}^{n} \frac{1}{c_{g_i}}} = \frac{N}{\sum_{i=1}^{n} \frac{1}{c_{g_i}}} \tag{3}$$

This straightforward derivation establishes that the average wave velocity is contingent not on the precise plate shape but on the thickness distribution. Furthermore, it underscores the necessity to rectify the commonly employed assumption that the average wave velocity serves as an accurate indicator of the average plate thickness. This is essential due to the markedly nonlinear relationship between thickness and propagation velocity. The average thickness and the standard deviation of the thickness distribution typically characterize the corroded plate's geometry. The average thickness facilitates the estimation of overall thickness reduction. However, while these parameters describe the entire plate surface, it doesn't imply that the same parameter set accurately characterizes each propagation path between the actuator and the sensor. As the plate surface becomes more irregular due to corrosion degradation, one anticipates more noticeable differences between individual propagation paths. The central concept presented in this study is not to ascertain the average thickness of the entire plate by solving an inverse problem, as demonstrated in [2122]. Instead, the focus is on comparing results obtained for specific propagation paths.

2.2. *Thickness variability influence on wavefront symmetry – Bilateral and rotational symmetry*

To evaluate the symmetry of the advancing wavefront, the initial imperative involves reconstructing its shape based on the signals recorded by the sensor network. The presented approach is usually used to assess the symmetry of expanding galaxies [28]. This necessitates the implementation of a specific procedure encompassing the following steps [20]:

1) Position the transducers equidistantly at distances denoted as r from the actuator and record the corresponding signals;
2) Identify the specific wave mode under consideration and ascertain its ToF;
3) Determine the lengths the wavefront propagates along by calculating velocities in particular directions. Subsequently, compute the distances travelled during the minimal ToF, utilizing the formula:

$$v_k = \frac{r}{ToF_k} \tag{4}$$

$$r_k = v_k \cdot \min\{ToF_i\} \tag{5}$$

where k represents the number of transducers, and i signifies the total count of transducers. The reconstructed wavefront manifests as a distribution over i arms, each of length r_k. This resultant configuration is denoted as M for subsequent analysis. The procedure of wavefront reconstruction is schematically presented in Fig. 3.

It should be noted here that the procedure of shape reconstruction is based only on the ToFs of incident waves measured by specific transducers. This significantly facilitate the whole procedure because we avoid measuring edge reflections which would significantly increase the difficulties of signals processing. On the other hand, the closely located damages like cracks or pits may affect the signals. If the localized damage would be positioned close to the sensor, the reflection would overlap with incident wave affecting its ToF. Because this study is focused on developing and testing the new procedure based on wavefront symmetry, we do not consider the possibility of additional reflections from other obstacles. However, this issue is crucial for the potential practical application of this procedure.

The assessment of corrosion-related degradation elucidated in this manuscript hinges upon scrutinizing bilateral and rotational central symmetry degrees. These symmetry measures are based on a series of geometric transformations for quantitative assessment of the symmetry of any shape. The concept of the symmetry measures is presented in Fig. 4 and was initially used for quantitative galaxy classification [28]. The procedure of symmetry assessment of propagating wavefield was presented in [20]. Consider a geometric shape denoted as M in the Euclidean space R^2.

Simultaneously, let M' represent the shape resulting from applying ith rotation operations to the original shape M. Similarly, M'' designates the shape achieved by reflecting shape M' across the specified x-axis. In defining the bilateral central symmetry degree, denoted as BCSD(i) concerning the x-axis, it is established as the ratio of the area designated as A (corresponding to the overlapping region between shape M' and its mirrored counterpart M'') to the total area occupied by shape M:

$$BCSD(i) = \frac{A\left(M_i' \cap M_i''\right)}{A(M)} \tag{6}$$

Furthermore, the bilateral symmetry of a given shape M is represented by δ_B, denoting the highest achievable value of the bilateral central symmetry degree:

$$\delta_B = \max\{BCSD(i)\} \tag{7}$$

This value falls within the range of 0 to 1, with 1 indicating a state of perfect bilateral symmetry within the shape. A systematic search can ascertain the count of axes exhibiting perfect bilateral symmetry, denoted as N_B. The number of axes representing imperfect bilateral symmetry is half of the discernible peaks in the BCSD function.

The rotational symmetry degree is defined as the ratio of the area of the intersection of the initial shape M and the rotated shape M':

$$RCSD(i) = \frac{A\left(M \cap M_i'\right)}{A(M)} \tag{8}$$

The maximum value of the rotational central symmetry degree, denoted as δ_R represents the rotational symmetricity of a shape M:

$$\delta_R = \max\{RCSD(i)\} \tag{9}$$

Since the value of RCSD is equal to 1 for an angle of 0 and 2π, which represent pseudo-data, they are to be discarded. The discarding procedure involves the following steps (Fig. 5):

1) Identify the first local minimum of RCSD denoted as l_1;
2) Identify the last local minimum denoted as l_2;
3) Discard the data close to 0 ($i < l_1$) and data close to 2π ($i > l_2$);
4) Determine the rotational symmetricity, taking into account the non-discarded data.

One can see, that in the case of the circular shape, both RCSD and BCSD would be equal to 1, regardless of the rotation angle. In the case of limited number of points used for shape reconstruction, corresponding

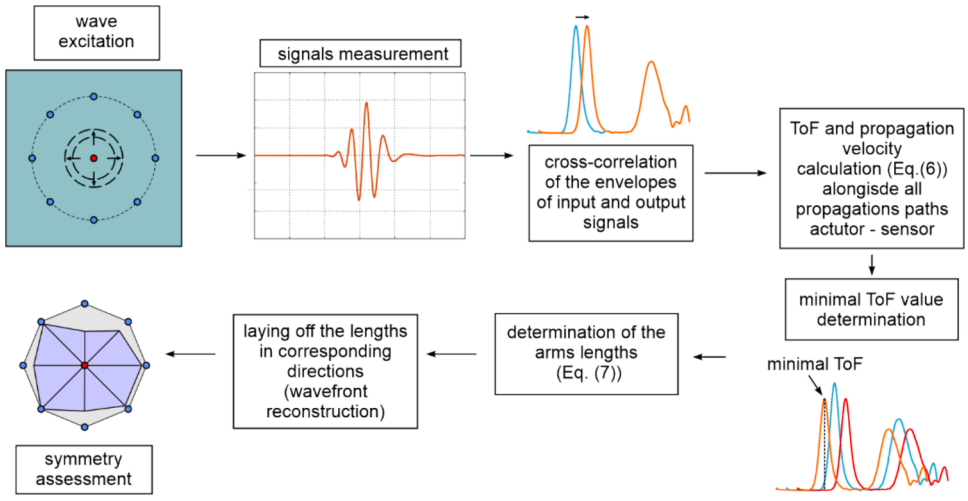

Fig. 3. The procedure of wavefront reconstruction based on ToF.

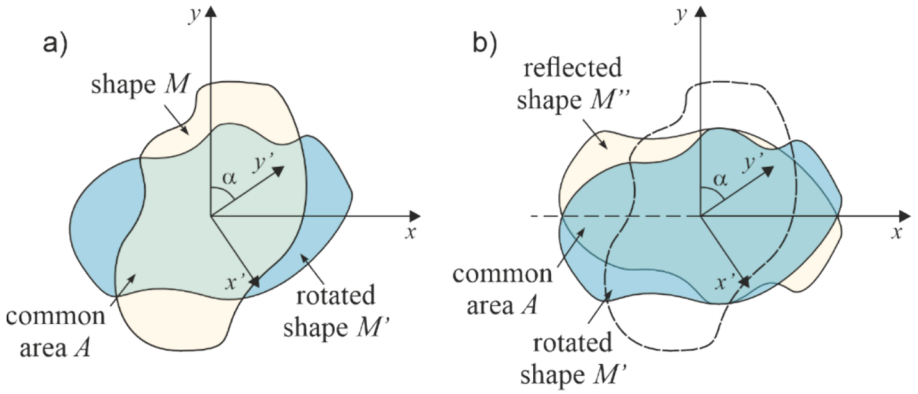

Fig. 4. The concept of a) bilateral and c) rotational symmetry: initial shape *M*, rotated shape *M*' and reflected shape *M*'' and common areas.

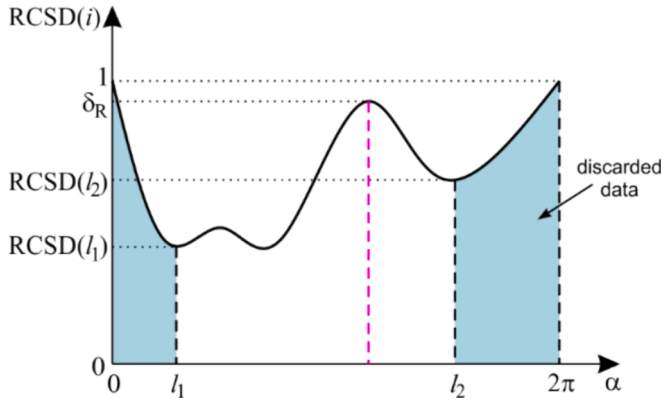

Fig. 5. Determining the rotational symmetricity from the RCSD plot [20].

to extent of transducers network, we obtain the figure with the number of vertexes equal to number of the transducers attached to the specimen surface (denoted as *i*). Then in the case of perfect symmetry and the equal ToFs for all sensors, the symmetry functions will have *i* local maxima equal to 1.

In the subsequent approach, it is assumed that a circular array of transducers will be employed. The significant uncertainty may arise due to the imperfect bonding of the transducers of the circular array to the plate, a concern to be adequately addressed in future investigations.

3. Materials and methods

3.1. Experimental tests

3.1.1. Plate models

Experimental testing was carried out on a square steel plate measuring 500 mm x 500 mm x 5 mm—typical thickness for applications in the shipping industry. Controlled corrosion was induced through electrolysis reactions, where ions were compelled to move by applying voltage from an external power supply. The plate, serving as the anode, was immersed in a 5 % sodium chloride solution, and a direct electric current (DC) was applied to hasten the corrosion process, with another metal bar acting as the cathode. The direction of the DC was carefully adjusted to optimize the corrosion conditions. The accelerated corrosion test continued for 240 h, after which the plate was removed from the solution and dried. Subsequently, nondestructive wave propagation tests were conducted on the corroded plate, followed by another round of electrolysis. To maintain consistency in the experiment, the sodium chloride solution was exchanged before each stage of the corrosion process, ensuring uniform electrolyte concentration. This procedure was iteratively repeated until the desired DoD was achieved. After the first round of accelerated electrolysis, the mass reduction was equal to 10 %; after the entire process, the mass was reduced by 20 %. Therefore, the results are collected for three different levels of degradation (0, 10 and 20 %). Fig. 6 provides a visual representation of the corrosion process in the steel plate.

The images clearly depict a substantial increase in the size and

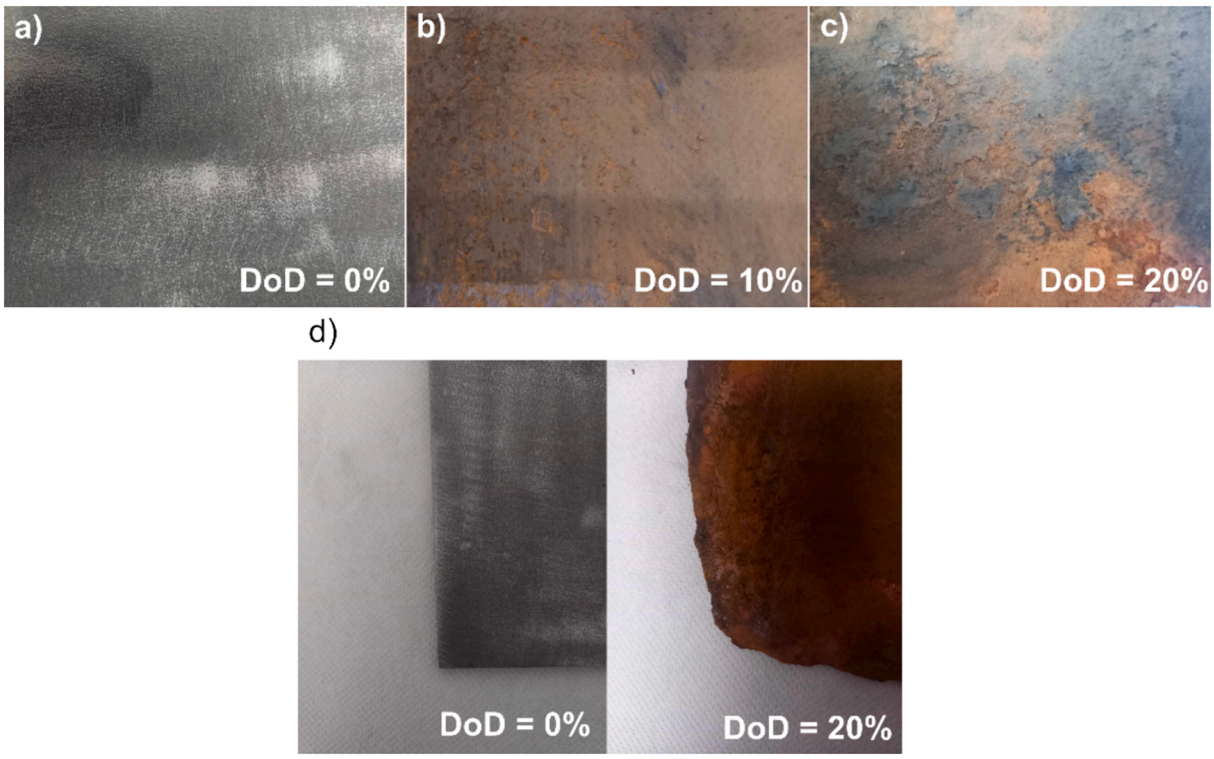

Fig. 6. The photographs of the experimental specimen characterized by a variable DoD: the plate with DoD of a) 0%, b) 10%, c) 20% and d) the comparison of the plate corners at the beginning and the end of the corrosion process.

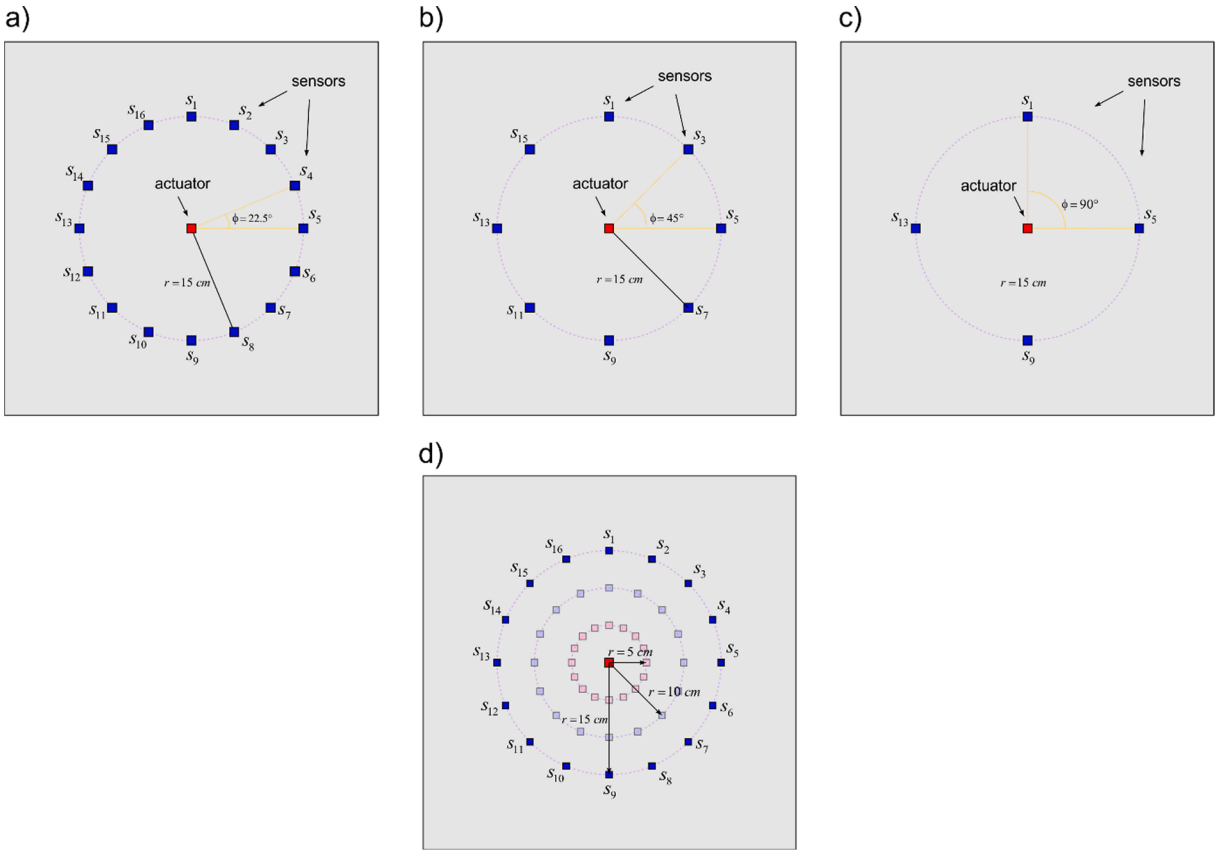

Fig. 7. Transducers configurations varying in number of sensors and the radius of the circular array tested during numerical and experimental campaigns: a) sensor network comprising of 16 transducers, b) 8 transducers, c) 4 transducers and d) investigated distances between excitation source and the sensors (5, 10 and 15 cm).

number of pits, signifying significant surface degradation. Additionally, photos of the plate corners at the beginning and end of the corrosion degradation process highlight the heightened susceptibility of corners and edges to corrosion.

3.1.2. Experimental equipment

The system employed for the experimental tests outlined in this study is depicted in Fig. 3. Guided waves were both excited and captured by piezoceramic transducers measuring 3 × 3 mm (NAC2024, Noliac). Operating in pulse-echo mode, these transducers were affixed to wax for stability. The excitation function p(t) was a five-cycle sine wave modulated by the Hann window, with carrier frequencies of 50, 100, or 150 kHz. The selection of these frequencies in detailed in the next section. An arbitrary function generator (TiePie) sent this excitation signal to the transducers connected with oscilloscopes (TiePie). Simultaneously, the sensors were connected to a high-voltage amplifier (Pendulum) to enhance the signal-to-noise ratio (SNR). The sampling frequency was of 10 MHz.

For the measurement of wavefront symmetry, a circular array consisting of 16 piezoelectric transducers was mounted on the plate surface (Fig. 7). Positioned on a circle with a 5, 10 and 15 cm radius. Each transducer was 5, 10 or 15 cm away from the wave source at the plate's middle point. The arbitrary circular configuration of the transducers was chosen to ensure accurate reconstruction of the wavefront shape. The necessity for precision in wavefront shape reconstruction drove the decision to use 16 transducers initially. In the following steps, the configuration of transducers was modified to verify the possibility of corrosion degradation monitoring using less extended sensor network. The wavefront was reconstructed using 16, 8, and 4 transducers. In total, 9 different configurations were tested (different radiuses of the circle on which sensors are mounted and different numbers of sensors). All cases are presented in Fig. 7d. The initial and the longest distance (30 cm) was determined by the test plate size (50 x 50 cm) and aimed to avoid the impact of edge reflections. In practical applications, such as ship and offshore structures, stiffeners can affect signal registration, necessitating a thoughtful adaptation of transducer spacing based on structural geometry and wave attenuation.

It is also noteworthy that the choice of plate size and sensor distance was influenced by the complexity and time duration of the numerical analysis detailed in the subsequent sections of the paper.

3.1.3. Nondestructive tests

The process of measuring the signal involved recording and averaging 300 consecutive signals. Following this, the averaged signal was applied to a five-order Butterworth band-pass filter with cut-off frequencies set at 20 Hz and 2f kHz, where f represents the excitation frequency [29]. This specific frequency range was selected to exclude any signal components outside of this band. To calculate the ToF of the first propagating mode, the up-sampled signals underwent auto-correlation. Peaks in the auto-correlated signals corresponded to ToFs, providing crucial information for the subsequent reconstruction of the wavefront shape.

The nondestructive tests were preceded by the selection of excitation frequency. To do this, the signals were collected for frequency range of 20 to 250 kHz and next, their SNRs were compared. The signals were easier to interpret for lower frequencies (up to 150 kHz). Above this frequency we noted also symmetric modes with relatively high-amplitude which hindered results interpretation. Because we wanted to test different frequencies varying in wavelength and the velocity, we decided to use 50, 100 and 150 kHz. The beginning of the dispersion curve for A0 mode is characterized by the greatest slope – for such selection one can expect the notable differences in propagation velocity. Nevertheless, the procedure of the optimal frequency choice requires further considerations and formulation of choice recommendations considering material parameters, initial plate thickness and the actual parameters of the irregular surface caused by environmental corrosion.

For numerical simulations, investigators directly specified the thickness variability. An exact reconstruction of the entire thickness variability observed in experimental models would be considerably more challenging. Nevertheless, two distinct approaches were used to assess thickness reduction during anodic dissolution. The total mass reduction was initially estimated by weighing the dried, corroded plate. This approach facilitated the estimation of the overall DoD using the expression:

$$DoD = \frac{m - m_{corr}}{m} \cdot 100\% \tag{10}$$

where m was the initial plate mass, and m_{corr} is mass reduced during electrolysis process. Subsequently, ultrasonic gauge measurements were carried out using a calibrated device manufactured by Metrison to determine thickness across a 50 mm mesh grid. A total of 121 measurements were conducted at each stage of the corrosion tests. The measurement grid is presented in Fig. 8.

The utilization of this ultrasonic measurement approach served two main purposes. Firstly, it adheres to the widely endorsed practice recommended by Classification Societies [4] for evaluating tangible corrosion degradation, especially in the context of ship hull diagnostics. Ultrasonic gauge measurements are crucial in generating maps of thickness variability, providing visual representations of general corrosion progression and non-uniform characteristics. Secondly, opting for this method enables a comparative analysis with the innovative approach focused on assessing wavefront symmetry in evaluating corrosion degradation.

3.2. Numerical study

3.2.1. Geometry of FE models – Random fields

We employed stochastic processes, specifically random fields, to simulate corroded surfaces. Given the random occurrence of pits, modeling their spatial distribution is effectively achieved through the random field approach—a method widely recognized for its suitability and robustness in handling an infinite set of spatially correlated random variables [30]. Random fields are mathematical functions spanning multi-dimensional spaces, incorporating pseudo-random values often accompanied by correctional elements. Various types of random fields, including Markov random fields (MRF), Gibbs random fields, conditional random fields (CRF), and Gaussian random fields (GRF), are available. Among these, Gaussian random fields are noteworthy for their characteristics, involving Gaussian probability density functions and the

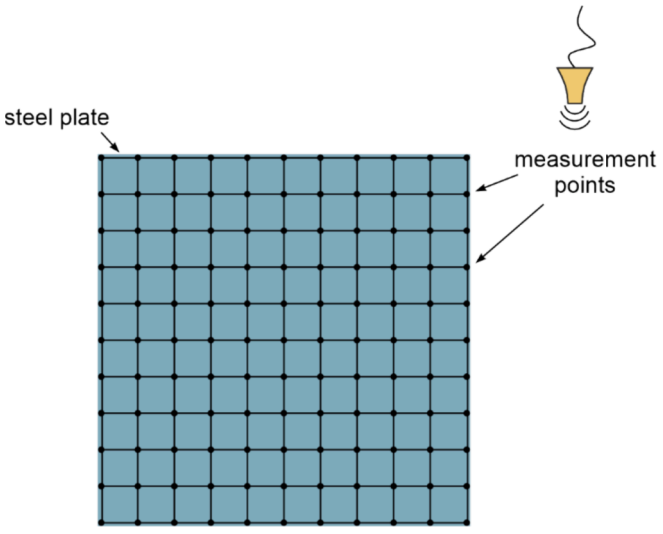

Fig. 8. Experimental investigation: the measurement grid for ultrasonic thickness determination.

ability to generate Gaussian free fields as distinctive instances. This results in irregular yet continuous surfaces across two-dimensional planes.

This study utilized random fields, specifically Gaussian random fields, to model the irregular surfaces of corroded plates. The MATLAB utility [31] facilitated our simulations, employing the Karhunen-Loeve (KL) expansion algorithm [32], which allows for the incorporation of user-defined parameters. Key considerations included specifying the random field's dimensions and initiating the process with a mesh measuring 100x100 units to ensure computationally feasible processing durations. Truncation, various levels of polynomial KL expansion, and the predetermined value dictating the interrelation between mesh points were also pivotal parameters. By carefully adjusting these parameters, we successfully simulated eroded surfaces by applying truncated Gaussian distribution within the overarching framework of random fields.

The numerical models considered in this study are outlined in Table 1. The initial thickness (d) of the plate was set at 5 mm, with adopted material parameters including an elastic modulus (E) of 210 GPa, density (ρ) of 7850 kg/m3, and Poisson's ratio (ν) of 0.3. The degree of degradation (DoD) varied from 0 to 60 %. For each DoD, various standard deviation values of thickness distribution were considered for random field generation, precisely, σ equal to 0.05, 0.1, 0.15, and 0.2 (Table 1). To explore the influence of excitation frequency, signals were collected at frequencies of 50, 100, and 150 kHz. In total, 63 models were examined, resulting in the processing of 1008 signals (refer to Table 1).

Due to the high stiffness of the actuator (115.00 N/μm), the actuation was simplified by applying a time-dependent concentrated force of 1 N at the middle point of the plate [33]. This simplification introduces local inaccuracies close to the excitation point, which is not a focal point in this study. The time course of the excitation aligned with experimental data, and signals were registered at selected model nodes corresponding to the exact positions of transducers during experimental tests. The compressive-type actuator predominantly induced transverse vibrations associated with A0 mode propagation, leading to the recording of the out-of-plane displacement component.

Numerical simulations were executed using the Abaqus/Explicit module. Despite the high computational cost, 3D models were employed as plain strain conditions would not allow modeling surface roughness and observing differences in wave propagation directions. The models utilized eight-node brick elements with reduced integration (C3D8R), and the transient wave propagation problem was solved with a time step of 10^{-8} s.

Table 1
Numerical models considered within the study.

Specimen group	Degree of degradation DoD [%]	Standard deviation σ
A#	0	0
B#	20	0.05
		0.1
		0.15
		0.2
C#	30	0.05
		0.1
		0.15
		0.2
D#	40	0.05
		0.1
		0.15
		0.2
E#	50	0.05
		0.1
		0.15
		0.2
F#	60	0.05
		0.1
		0.15
		0.2

3.2.2. Parameters of numerical models

We conducted numerical simulations using the commercial software Abaqus, utilizing the Explicit module to solve the transient wave propagation problem. The plates were modeled as 3D objects constructed with 8-node brick elements featuring reduced integration (C3D8R). The time step and element size were adjusted according to the excitation frequency range and wavelength to meet the Courant- Friedrichs- Lewy conditions. The element size was limited not to exceed 0.5x0.5x0.5 mm^3, and the time step was set at 10^{-8} s. The analysis duration was 0.5 ms. Excitation was applied as a time-dependent force at the plate's middle point. Fig. 7 illustrates the numerical model with the applied load, and the excitation function took the form of a five-cycle sine modulated by the Hann window:

$$p(t) = \begin{cases} 0.5p_0 \sin(2\pi ft)\left(1 - \cos\left(\frac{2\pi ft}{n_w}\right)\right) & t \in [0, T_w] \\ 0 & t \geq T_w \end{cases} \quad (11)$$

where f denotes the excitation frequency, the excitation amplitude, the Hann window length, and the number of time steps; material parameters adopted in the model were typical for steel specimens and were as follows: elastic modulus $E = 210$ GPa, Poisson's ratio $\nu = 0.3$, and density $\rho = 7850$ kg/m^3. The numerical simulations for the 3D model were performed to reflect the surface roughness caused by corrosion degradation (Fig. 9).

Each plate was also tested by applying variable frequencies (50, 100, and 150 kHz). Additionally, three different sensors network extends, and three different radiuses of the circular array have been investigated. In total, the numerical simulations have been performed for 567 plate models.

4. Numerical results

4.1. The influence of DoD on wavefield symmetry

In the initial phase of the analysis, we analyze the impact of the average mass loss on the shape of the wavefront [34]. Fig. 10 illustrates the field of wave propagation at specific time points for plates with varying DoD. These snapshots correspond to three models A#, B#, and D#, sharing the same standard deviation of thickness distribution and a representative frequency of 100 kHz. The visual representation unmistakably highlights the influence of corrosion degradation on the advancing wavefront.

Two main observations emerge from this analysis. Firstly, as the DoD increases, the circular symmetry of the wavefront diminishes. This effect is visible for wave propagation velocity, as well as for the amplitude. The wavefront maintains circular symmetry in an ideal, undamaged isotropic plate with constant thickness, given that the wave propagates uniformly in all directions. However, in the case of damaged plates with variable thickness, the propagation paths exhibit varying velocities, disrupting the circular symmetry. Additionally, there's an associated effect concerning the area covered by the wavefront. The reduction in thickness leads to a decrease in propagation velocity, resulting in shorter propagation paths. This effect is also crucial for the investigations on the influence of general corrosion on the time of flight and in consequences on the all algorithms based on this parameter i.e. algorithms of point-like damage detection.

The influence of corrosion damage on the ToF is also visible in measured signals. In Fig. 11 the signals collected from analyzed plates are illustrated and the incident waves were identified and highlighted. Only signals from four sensors positioned at 90-degree intervals (sensors 1, 5, 9, and 13) are presented in the graph to enhance clarity. As mentioned earlier, in the scenario of an undamaged plate, the graph reveals the ideal symmetry of the advancing wavefront. The signals depicted in Fig. 11a coincide perfectly, displaying identical time courses and amplitudes for respective wave packets. Conversely, signals

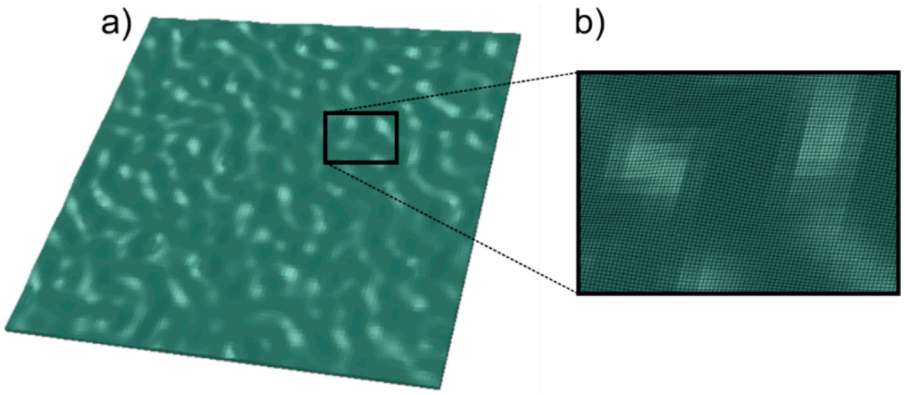

Fig. 9. Numerical simulations performed in Abaqus software: a) model of the corroded plate, b) zoom of the plate surface.

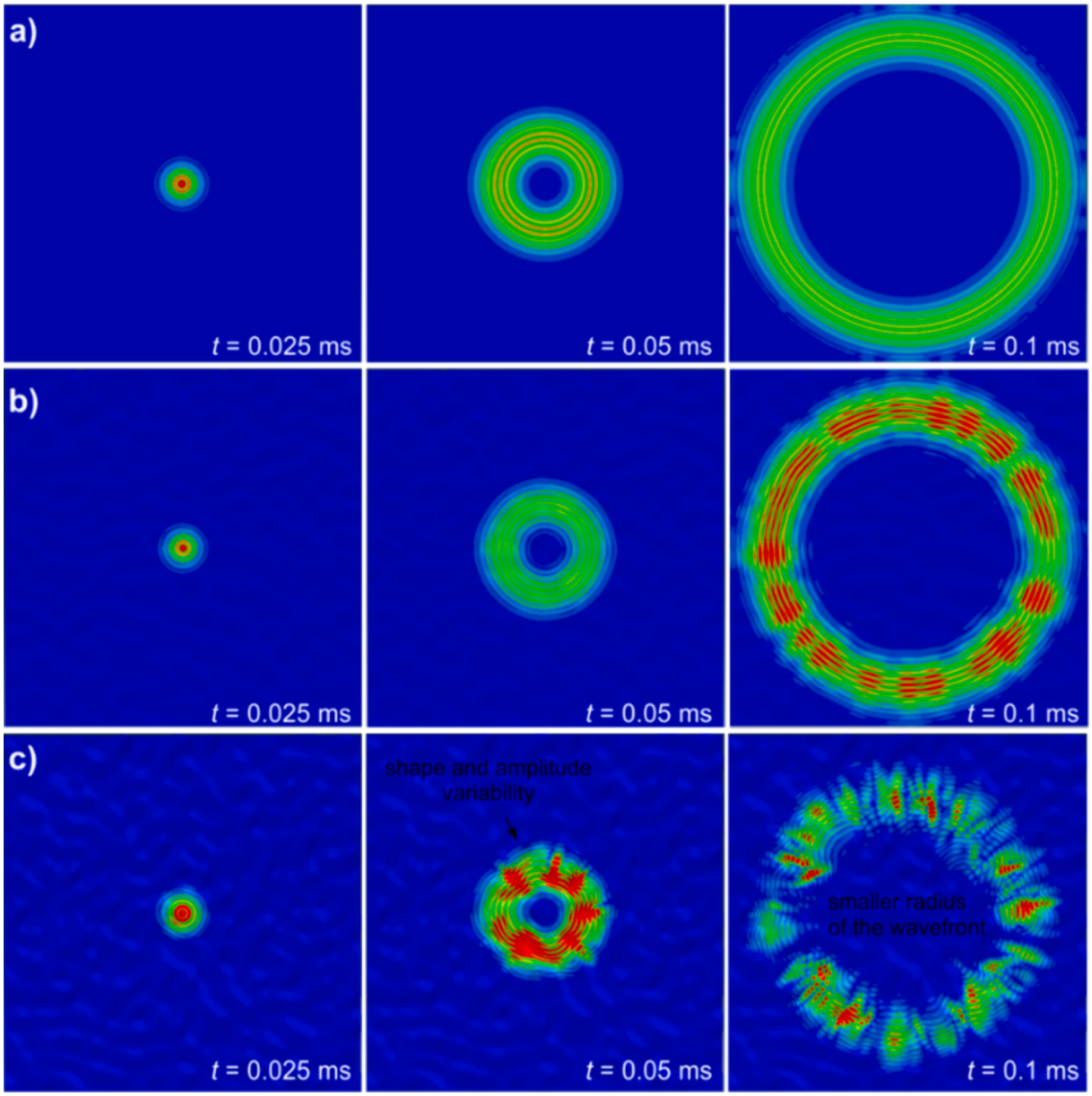

Fig. 10. Visualization of wave propagation in steel plates varying in DoD: a) undamaged plate, b) plate with DoD of 20%, and c) plate with DoD of 40%.

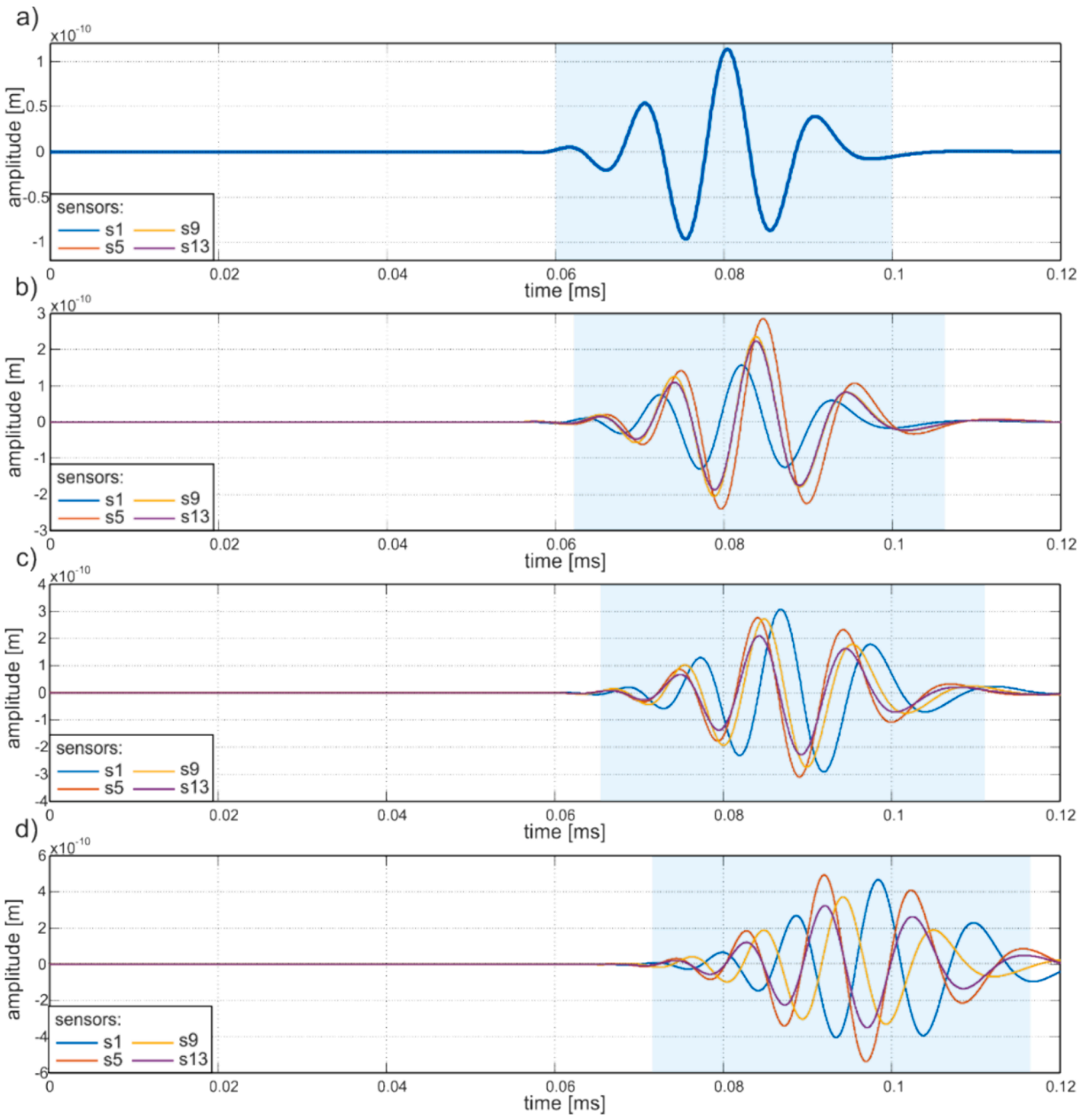

Fig. 11. Exemplary wave propagation signals obtained for variable DoD: a) DoD = 0 %, b) DoD = 20 %, c) DoD = 40 % and d) DoD = 60 %.

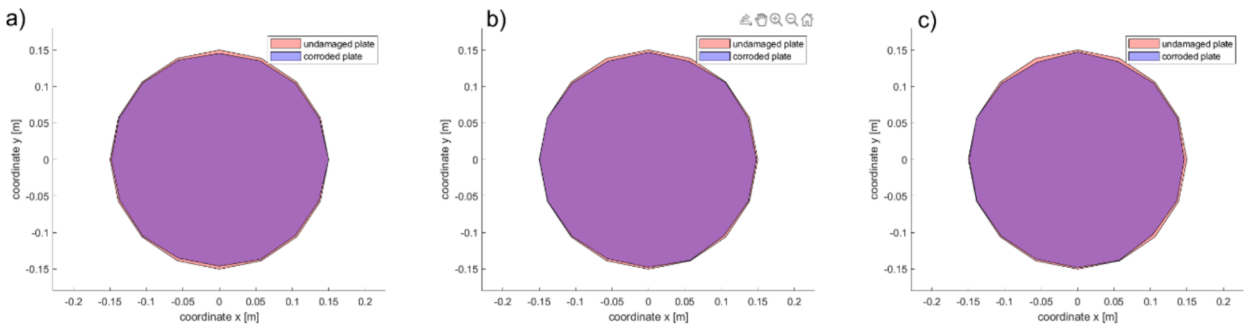

Fig. 12. Exemplary reconstructed wavefronts for variable DoD (in each case, the excitation frequency was equal to 150 kHz, and the standard deviation of thickness distribution was 0.15): a) DoD of 20 %, b) DoD of 40 % and DoD of 60 %.

obtained from corroded plates exhibit variations in the ToF of individual wave packets. Despite the DoD and the standard deviation of thickness distribution being defined across the entire plate, the ToF and signal characteristics differ in various directions. Moreover, one can see that the average ToF of measured signals also differs with increasing DoD. For chosen excitation parameters, the ToF increases, which corresponds to the visualizations presenting a decreasing size of the spreading wavefront. This observation supports the central premise of our study, emphasizing that corrosion degradation not only impacts the average wave propagation velocity due to thickness reduction but also disrupts the symmetry of wave motion within the plate.

The acquired signals underwent processing following the method detailed in Section 2.2, and the resulting wavefront shapes were reconstructed, as depicted in Fig. 12. The red-marked shape corresponds to the wave propagating in the undamaged, smooth plate, while the purple represents a wave spreading in the corroded plate. Despite potential overlapping due to the smaller area covered by the purple shape in each case, it is noticeable that the purple wavefront is consistently characterized by a reduced area compared to the red one. However, relying solely on visual assessment to discern the corrosion degradation process by comparing wavefronts for plates with varying DoD would be challenging. The differences in specific wavefront shapes appear insignificant, making it difficult to discern the extent of corrosion degradation based solely on visual inspection.

Investigating the impact of DoD on wavefront symmetry degrees involved a quantitative analysis. In the forthcoming figures, we illustrated the RCSD in Fig. 13 and the corresponding BCSD functions in Fig. 14. The central symmetry functions were determined and presented for clarity and simplicity at the outset. Subsequent sections will focus exclusively on maximal and minimal symmetry degrees. The outcomes for frequencies ranging from 50 to 150 kHz are organized in columns, while variable DoD results are presented in rows. Because the tendency is clearly visible in the figures, we introduced the functions only for three different DoDs (plate B#, D#, #F). Each graph displays four functions, each corresponding to a distinct standard deviation of thickness distribution. A discernible trend emerges, showcasing the substantial influence of DoD on symmetry degree functions. Both BCSD and RCSD functions exhibit reduced values with increasing DoD. Notably, in the case of BCSD, irregularities become apparent, as illustrated in Fig. 14a and c. Moreover, one can see that both types of symmetries can be efficiently used for corrosion monitoring.

The maximum and minimum values of RCSD and BCSD functions have been extracted and are presented as graphs in Fig. 15. Because the symmetry functions demonstrated similar capabilities for all frequencies (50 100 and 150 kHz), the degrees were determined only for 100 kHz. Additionally, we identified the theoretical minimum and maximum symmetry degrees for each scenario in pristine, undamaged plates. The figures indicated their values in straight dashed lines: a grey line labeled A for minimal values of BCSD, a green dashed line labeled B for maximal values of BCSD, a pink dashed line for minimal values of RCSD, and a purple line D for a maximum value of RCSD. In undamaged plates, the maximum symmetry value consistently equals 1, signifying that the rotated and/or reflected shape precisely aligns with the initial wavefront shape. However, the minimum value is contingent on the number of sensors within the network, increasing in tandem with the network extent. In the case of a 16-sensor network, the minimum value is determined to be 0.993. Regardless of which type of symmetry degree (minimum or maximum) and the type of symmetry (rotational or bilateral), we can observe the decrease of the proposed indicator with the deterioration of the plate state. The decrease is more significant for plates characterized by the greater standard deviation of the thickness distribution. The augmentation of the standard deviation leads to heightened variability of the plate thickness and, in consequence, in wave propagation velocity, resulting in lower symmetry degree values. Furthermore, this impact becomes more pronounced, particularly with larger DoD. The symmetry degrees obtained for DoD of 20 % (left side of each graph) are very similar regardless of the standard deviation. The case of DoD equal to 60 %, the difference between both types of symmetry degrees (right side of each graph) is much more noticeable. One can conclude that not only the level of degradation but also the surface roughness influences wavefront symmetry.

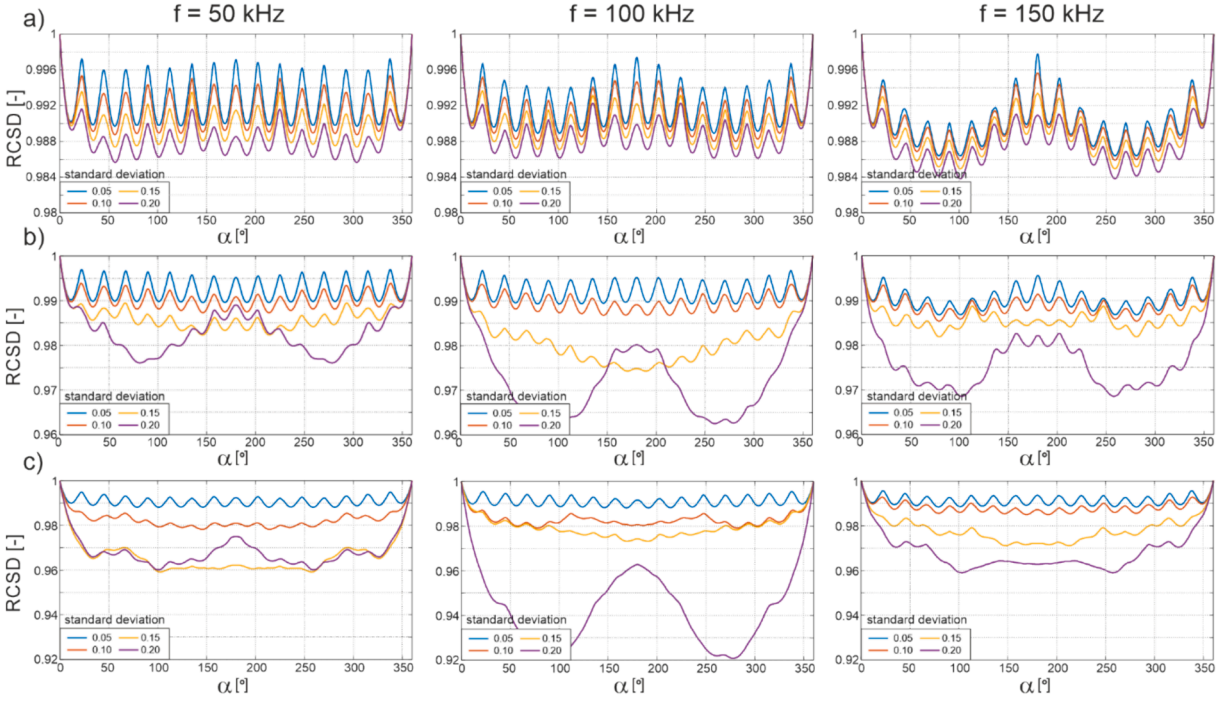

Fig. 13. RCSD functions determined for plates varying in DoD: a) 20%, b) 40%, c) 60% obtained for different excitation frequencies and standard deviations of thickness distribution.

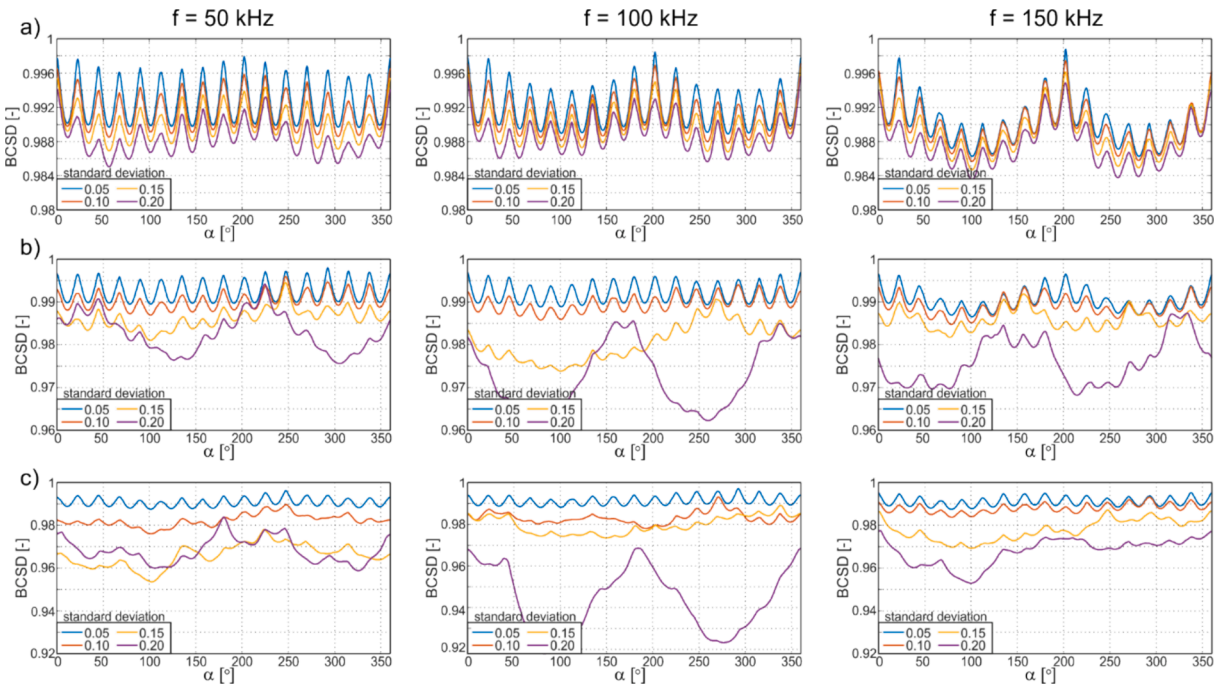

Fig. 14. BCSD functions determined for plates varying in DoD: a) 20%, b) 40%, c) 60% obtained for different excitation frequencies and standard deviations of thickness distribution.

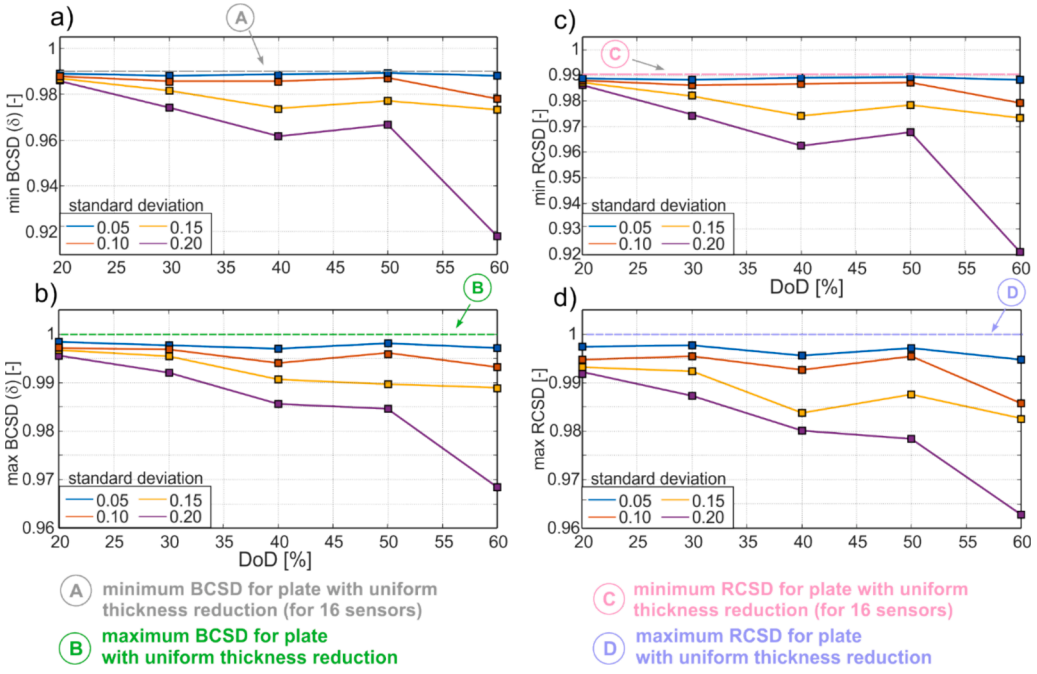

Fig. 15. Extreme values of BCSD and RCSD functions determined for plates varying in DoD: a) minimal values of BCSD, b) maximum values of BCSD, c) minimal values of RCSD and d) maximum values of RCSD.

4.2. The influence of the number of sensors on obtained symmetry functions

In the next stage, the symmetry degrees were determined for the variable number of sensors in the network. One can expect a reduction in the accuracy of the wavefront shape reconstruction. However, the extent of the sensor network influences the cost of the potential monitoring system and the amount of data that has to be processed. Fig. 16 presents the symmetry degrees determined for variable DoD for increasing extent of the sensor network: 4, 8 and 16 sensors. Because the tendency for other indicators, i.e., minimum and maximum values of RCSD and BCSD, as well as for different frequencies, was the same, we present the results only for the maximum values of RCSD and for excitation frequency 100 kHz.

As anticipated, fewer sensors corresponded to diminished conclusiveness in the obtained results. An initial observation in the network incorporating four sensors (Fig. 15a) revealed an escalation in the RCSD function with increasing DoD. Specifically, across all standard deviation

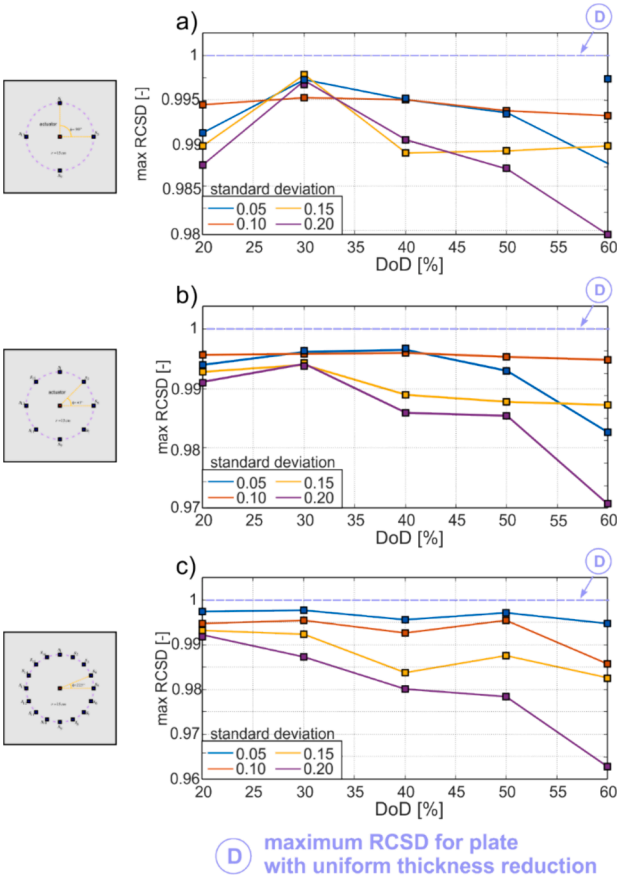

Fig. 16. Maximum values of RCSD obtained for a variable number of transducers in the network: a) results for 4 transducers, b) 8 transducers and c) 16 transducers.

values, the RCSD associated with a DoD of 30 % exceeded that of a DoD of 20 %. Subsequently, as the degradation progressed, the degree of symmetry exhibited a declining trend in nearly all instances. Notably, a divergent increasing trend was once again discerned for a plate characterized by a relatively high standard deviation in thickness distribution (0.15, denoted by the yellow line).

Furthermore, in the scenario involving a more comprehensive sensor network encompassing eight sensors (illustrated in Fig. 16b), an upward trajectory in the degree of symmetry was also discerned with escalating degradation levels. Notably, these changes did not manifest as abrupt peaks. Despite the most unequivocal outcomes being obtained for the highly extensive sensor network (depicted in Fig. 16c), it is evident that a less extensive network with eight sensors can still afford satisfactory quality monitoring of corrosion progression. The subsequent sections of the paper will delve into the discussion and description of additional plans to enhance the accuracy of corrosion level assessment.

4.3. The influence of the distance between the actuator and sensors on the wavefield symmetry assessment

The subsequent phase was directed towards scrutinizing the impact of the spatial arrangement of sensors, a pivotal aspect for optimizing sensor placement. The delineated wavefront reconstruction methodology was formulated to augment the evaluation of corrosion degradation in extensive plate-like structures using ultrasonic measurements, notable for their efficiency and temporal reliability. Consequently, an optimal scenario involves surveilling a maximal surface area within a single measurement, prompting the placement of sensors along a circular trajectory with a substantial radius for monitoring expansive regions. Conversely, the corrosion monitoring approach predicated on symmetry assessment, as presented herein, lacks granularity in detailing the thickness distribution. Consequently, a generous radius of the circular sensor array provides only coarse insights into the degradation within the monitored area. Furthermore, the underlying assumption of wavefront asymmetry measurement is contingent upon variations in wave propagation velocity induced by variable thickness. For propagation paths traversing corroded plates characterized by statistical descriptors, the differences may be mitigated over sufficiently long paths, converging towards the descriptors of the plate surface. In such instances, a symmetrically reconstructed wavefront could lead to underestimation or even non-detection of corrosion degradation. Alternatively, very short propagation paths may exhibit substantial differences in parameters, such as average thickness and standard deviation, diverging from the overall descriptors of the plate surface due to the presence of deep corrosion pits.

Considering a relatively short radius for the circular array of sensors enables more precise plate assessment, albeit with an attendant increase in the requisite number of measurements and data processing workload. In such cases, the proposed methodology aligns in temporal investment with conventional ultrasonic measurements. Additionally, shorter propagation paths correspond to lower ToF for signals, where even minor variations in ToF among sensors may approach the measurement error, potentially induced by imprecise sensor installation. Inconsequential differences in ToF could manifest as elevated symmetry degrees in the wavefront.

These considerations underscore the imperative need to account for the influence of sensor placement on the derived results. Fig. 17 illustrates the maximum values of RCSD and BCSD for varying numbers of sensors organized in circular arrays with different radii. It is evident from the results that the efficacy of the corrosion monitoring process is more significantly impacted by the number of sensors in the network rather than the spatial separation between them.

The essential conclusions concern the corrosion indicators: the results obtained for variable number and configuration of sensors indicate that the more unambiguous decreasing trend with increasing DoD was noted for rotational symmetry degree marked by the blue solid line. In the case of bilateral symmetry degree, the localized peaks were observed even of the DoD increased. However, the radius of the circular array had less influence on the determined relationships between symmetry degrees and the DoD. Their characteristics are similar regardless of whether the radius of the array was equal to 5 or 10 cm. The clear decreasing trend of both types of symmetry degrees was obtained for each length of the radius in the case of the most extensive network comprising of 16 sensors (see Fig. 17 – third row). We can state that the proposed method works well for various sizes of the monitored area if the wavefront is reconstructed with sufficient accuracy.

5. Experimental results

5.1. Thickness measurements

One key limitation of experimental tests that involve anodic dissolution is the inherent challenge of enforcing a specific standard deviation in thickness distribution. Therefore, the experimental results are presented only for a limited number of cases. As mentioned, the accelerated corrosion process was conducted in several stages, and the measurements were made after reaching the desired DoD level. However, the standard deviation of the thickness distribution was not possible to control and modify. The plate surface morphology was investigated by using an ultrasonic thickness gauge and the parameters of corroded plates are added for readers' information. Moreover, in Fig. 18, thickness maps obtained through the standard ultrasonic gauge approach are illustrated. A noticeable decrease in thickness is observed, particularly at the edges of the plate, which is a common effect. Since the sensors are positioned in the middle section of the plate, the wavefront is

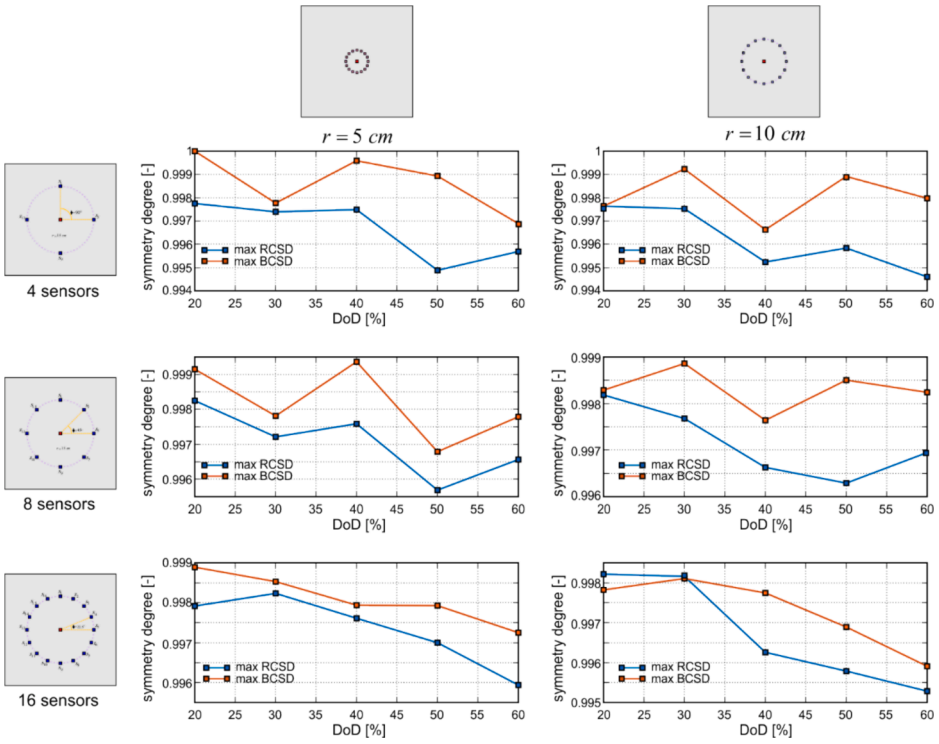

Fig. 17. The maximum values of RCSD and BCSD collected for a variable number of sensors organized in circular arrays with different radiuses (rows present the results for a variable number of transducers while columns contain the results for different radii of the array).

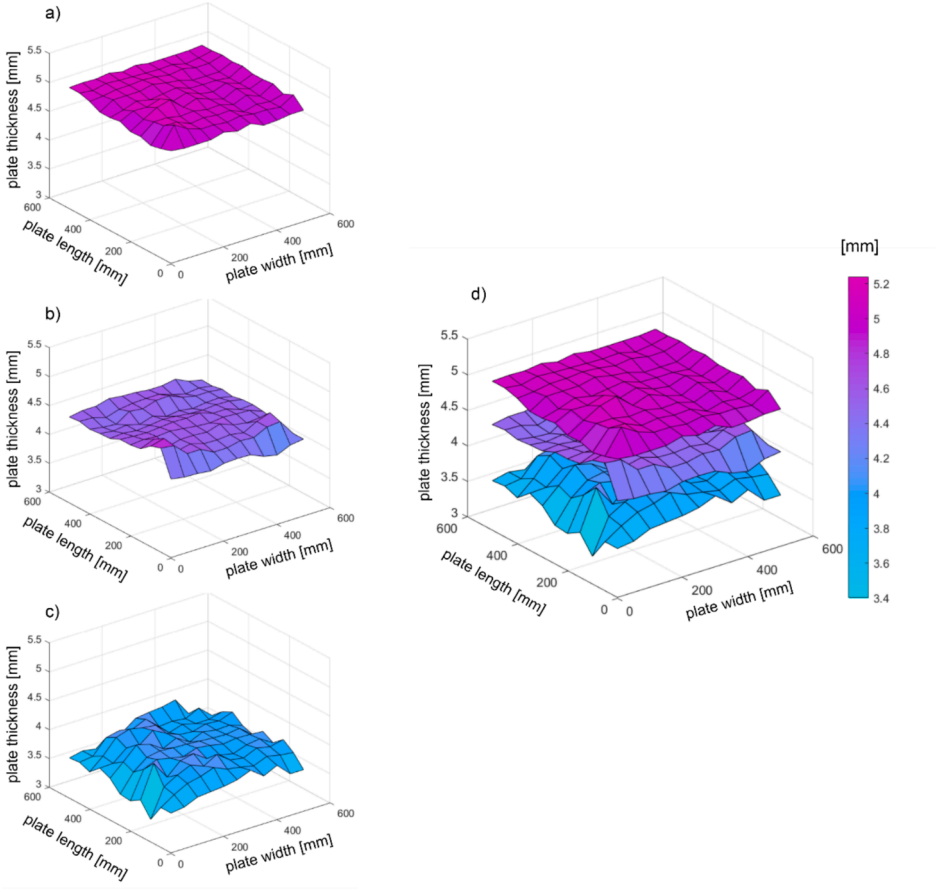

Fig. 18. Thickness map obtained during ultrasonic measurement: a) intact plate, b) plate with DoD of 10%, c) plate with DoD of 20% and d) comparison of all performed thickness maps.

exclusively influenced by thickness irregularities in this region. Consequently, the reduction in thickness at the plate edges does not impact the measured signals. The significant reduction of the plate thickness and edges is also the main reason for terminating the experimental research after obtaining the DoD of 20 %. The further anodic dissolution would lead to deterioration of the plate edges and dissolution of the corners rather than the entire plate surface. Therefore, we decided not to investigate the specimens which were considered to be unrepresentative.

Based on the ultrasonic measurements, the average thickness and the standard deviation of the thickness distribution have been determined at each stage of the experimental tests. The intact plate had a thickness of 5.046 mm, and the standard deviation was 0.046. Even for the DoD of 0 %, the plate surface was not perfectly flat, which is also visible in the thickness map (Fig. 18a). After the first stage of anodic dissolution, the DoD was about 10 %, the average thickness was 4.501 mm, and the standard deviation increased and was equal to 0.100. The corrosion process was terminated after reaching the DoD of 20 % and at this time the average thickness was 3.945 mm and the standard deviation was 0.143. One can see, that due to progressive corrosion degradation not only the mass reduction was observed but also the plate surface became more rough. Therefore, It is justified to test various combinations of statistic parameters and their influence on wave propagation as they can change during corrosion.

The experimentally measured signals for variable DoD have been compared in the first step. The selected results of the wave propagation campaign in corroded plates are presented in Fig. 19 [34]. As previously, the figure contains the results for selected sensors and for one frequency (100 kHz) to avoid the deterioration of the readability of the graphs. The plots were prepared for sensors s1, s5, s9 and s13. The discrepancy between theoretical predictions and experimental measurements arises from the imperfect match in signals recorded for the undamaged plate. In the numerical model, signals at the same distance from the actuator were identical, while experimental tests, though notably similar, displayed observable differences in amplitude and ToF. These disparities are attributed to variations in transducer attachment methods. In the experiments, wax was utilized for its advantage in easy removal before immersion and accelerated corrosion. However, wax quantity and temperature impacted signal amplitudes, leading to differences. Another factor contributing to signal variation was the precision of transducer attachment, despite meticulous efforts. Measurement tools, such as a tape measure, introduced a potential for subtle deviations in sensor locations. Additionally, even when structurally sound, geometric irregularities in the undamaged plate resulted in thickness variations, potentially introduced during the initial cleaning and polishing stages. As a result, ToF measurements at different locations may exhibit slight discrepancies. As the DoD increases, the differences in signals become more evident. In the case of DoD of 20 % (Fig. 19c), The most significant differences in ToF and the amplitude are observable, which is associated with the highest asymmetry of the propagating wavefront.

The collected signals have been processed to determine the RCSD and BCSD functions presented in Fig. 20. The functions were plotted for the most extensive sensor network, comprised of 16 transducers localized 15 cm from the actuator, to demonstrate the influence of DoD on the wavefront symmetry. The function values generally decreased with increasing DoD, regardless of the excitation frequency and the type of symmetry (bilateral or rotational). The extracted maximum and minimum values of BCSD and RCSD, considered corrosion level indicators here, are collected in Fig. 21. The corrosion degradation inevitably influences the wavefront symmetry, manifested by the decreasing trend of the extreme values of the symmetry functions. The colored dashed lines denoted by A, B, C and D indicate the extreme values of the symmetry degrees obtained theoretically for the network comprised of 16 transducers. As one can see, the theoretical value of the degree of symmetry is always higher than the experimental one. It can be explained by the fact that perfect symmetry is usually difficult to obtain in natural conditions.

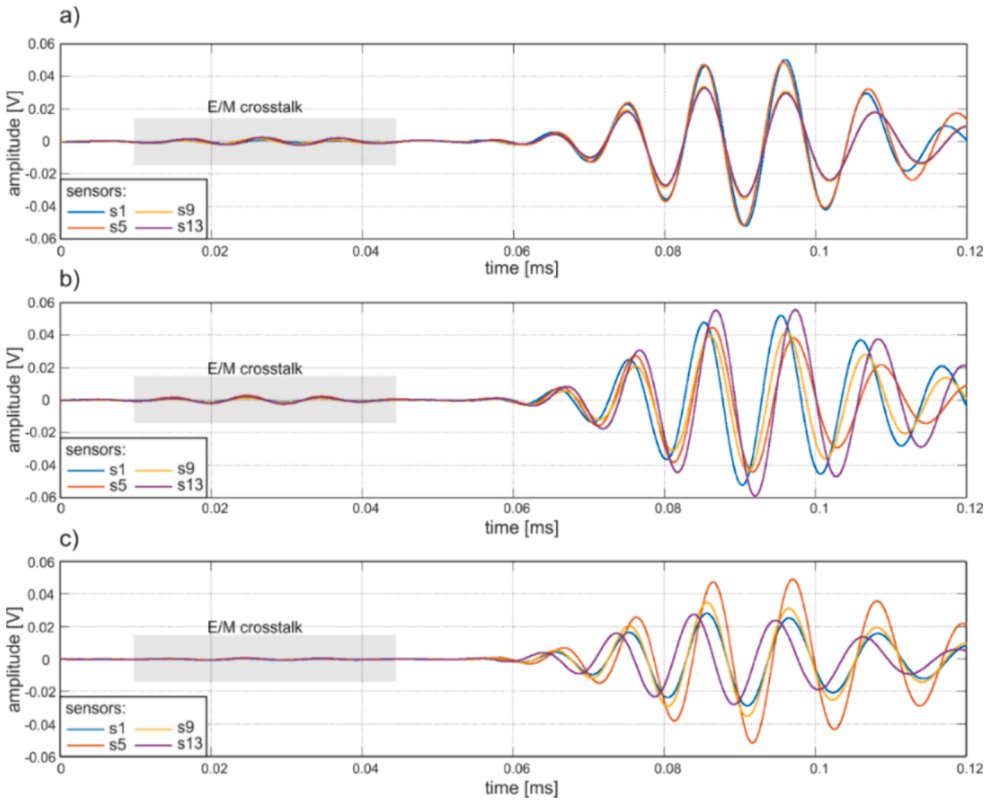

Fig. 19. Wave propagation signals registered by the four sensors of circular array attached on the plate characterized by variable DoD: a) DoD of 0%, b) DoD of 10% and c) DoD of 20%.

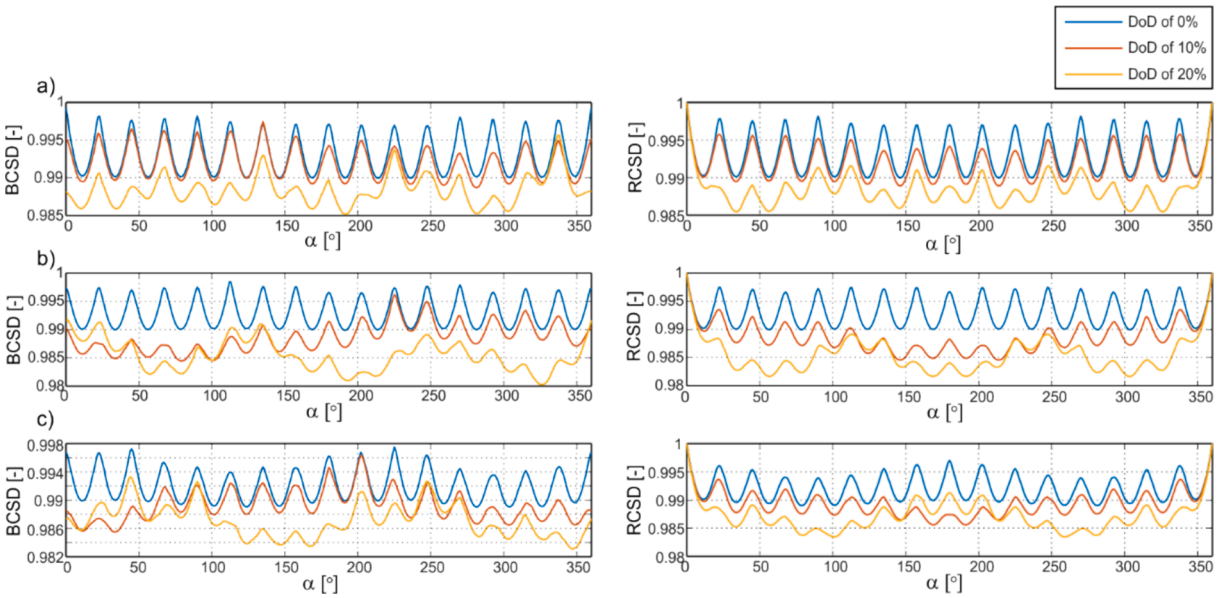

Fig. 20. BCSD functions (left column) and RCSD functions (right column) determined for experimental plate characterized variable DoD and for different excitation frequencies a) 50 kHz, b) 100 kHz and c) 150 kHz.

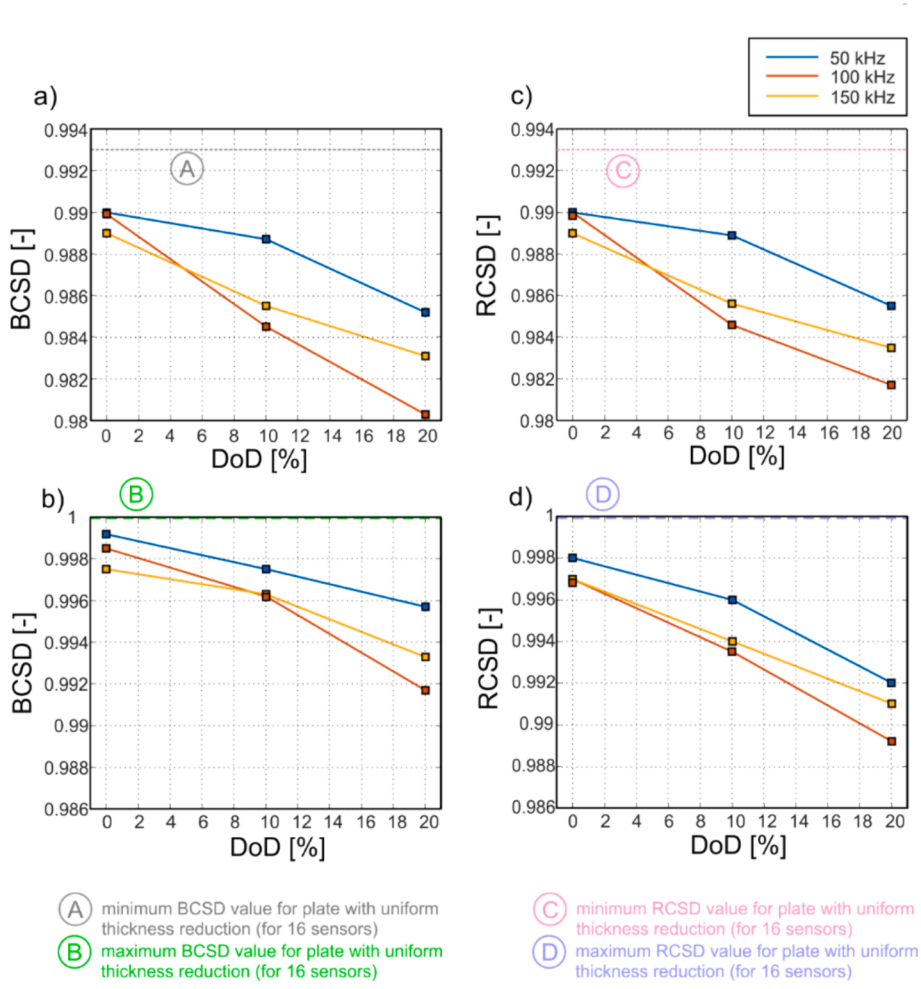

Fig. 21. Experimentally obtained extreme values of BCSD and RCSD functions determined for plates varying in DoD: a) minimal values of BCSD, b) maximum values of BCSD, c) minimal values of RCSD and d) maximum values of RCSD.

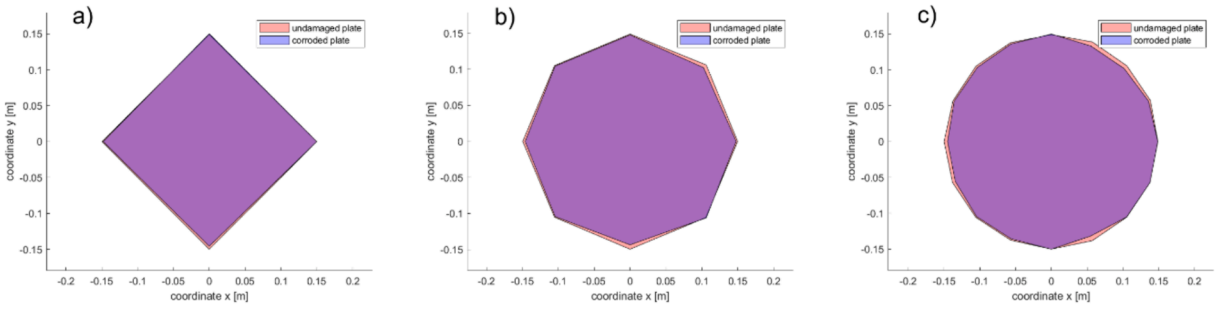

Fig. 22. Wavefront shapes obtained for a variable number of sensors in the network (reconstruction made based on results obtained for a plate with DoD of 20%): a) 4 sensors, b) 8 sensors and c) 16 sensors.

5.2. The influence of the number of sensors on obtained symmetry functions

Next, the influence of network extent was investigated. To demonstrate the accuracy of the wavefront shape reconstruction obtained for various numbers of sensors in the network, the wavefronts determined for DoD of 20 % and for excitation frequency of 100 kHz have been depicted in Fig. 22. The number of corners corresponds to the number of transducers. In each case, the wavefront determined for the undamaged experimental plate for comparison was also added. It is evident that regardless of the number of sensors, the difference between the wavefronts for health and the corroded plate is insignificant, even though the DoD was relatively high and was over 20 %. By reflecting and/or rotation, the symmetry degrees of the particular wavefront were determined, and then the extreme values of RCSD and BCSD were extracted (Fig. 23). The decreasing trend of symmetry degrees was noted for all extents of the transducer network. Despite that, the monitoring process based on bilateral symmetry (Fig. 23b) would be more challenging due to the insignificant reduction of the degree of symmetry for progressive deterioration of the tested plate. The maximum value of BCSD obtained by the sensor network comprising of 4 transducers varied from 0.999 to about 0.997 for mass reduction equal to 20 %. Despite the decreasing trend of this indicator, its variability is comparable to the measurement error. For the greater number of transducers, the decrease was more noticeable but still insignificant (the drop from 0.999 to 0.994 for 8 sensors and from 0.998 to 0.992 for 16 sensors). Nevertheless, the most significant indicator reduction was observed for the most extended network. More noticeable differences in indicators for variable DoD were noted for rotational symmetry. Moreover, the slope of the curves representing the DoD-max RCSD relationship was comparable regardless of the number of sensors used for monitoring, which suggests that the proposed approach can be suitable even in the case of a less extensive measurement system.

5.3. The influence of the distance between the actuator and sensors on the wavefield symmetry assessment

The last stage of the research concerns the variable actuator-sensors distance analysis. The comparison of the experimentally determined highest symmetry degrees collected for different DoDs is presented in Fig. 24. As in the case of numerical results collected for the higher number of cases, one can see that the efficacy of the corrosion monitoring process is more dependent on the number of sensors in the network rather than the spatial separation between them. The decreasing trend of the considered symmetry degrees with increasing DoD was noted for all transducer configurations. Both numerical and experimental results indicate that the investigator can adjust the size of the monitored area depending on the current needs. However, again, the number of sensors seems crucial in analyzing the wavefront asymmetry. It should be noted here that in some cases, the degree of symmetry remained the same or even increased when the DoD increased from 10 %. The apparent drop of the symmetry degree value was observed only for the network built of 16 transducers.

6. Conclusions and discussions

The last section is devoted to a discussion of the results presented, with particular emphasis on the limitations of the method presented and potential future work to be carried out.

The paper presents the results of numerical and experimental investigations on the influence of corrosion degradation on wavefield symmetry. Because the proposed procedure assumed the reconstruction of the wavefront shape by processing the collected signals' wavefronts, we also analyzed the influence of their number and distance between

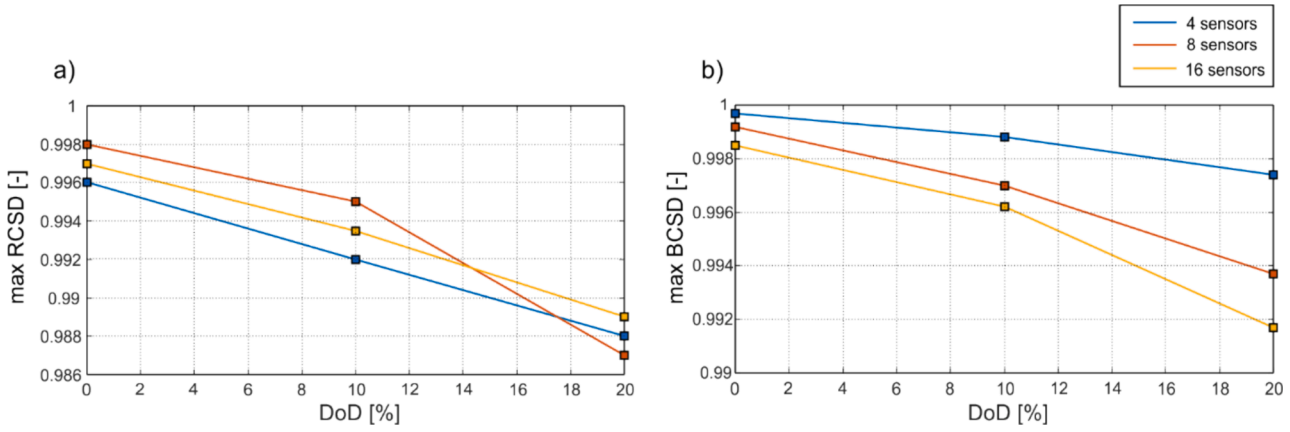

Fig. 23. Maximum values of a) RCSD and b) BCSD functions obtained for variable DoD (experimental tests conducted for variable number of the transducers attached 15 cm from the actuator).

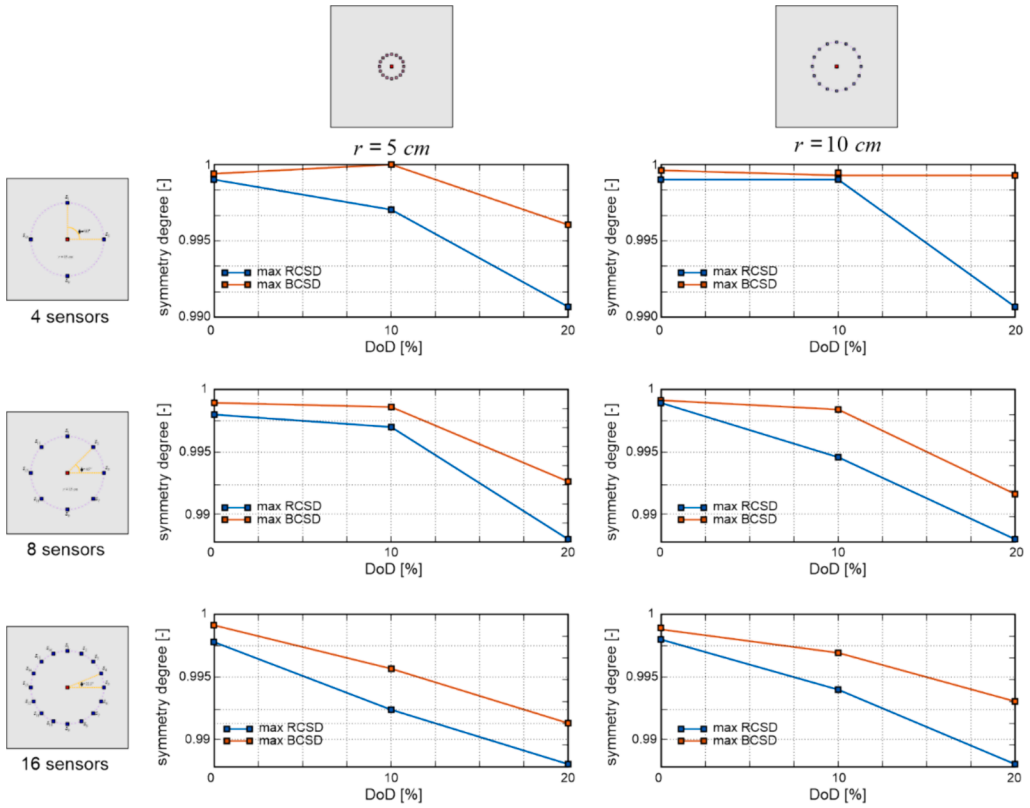

Fig. 24. The maximum values of RCSD and BCSD collected during the experimental campaign for a variable number of sensors organized in circular arrays with different radiuses (rows present the results for a variable number of transducers while columns contain the results for different radii of the array).

them on the accuracy of the wavefront shape determination and indirect corrosion monitoring. This is crucial for the further development of the novel devices used for state assessment of plate-like structures. The increase of number of sensors, except the higher cost of the system, entails increasing installation time. Also, the possibility that any sensor will be installed incorrectly is higher, which is absolutely pivotal in wavefront symmetry assessment. On the other hand, the greater number of signals measured, the more information about the structure we have and the more precise wavefront we can reconstruct. The same situation applies the distance between sensors. The larger the distance, the greater area we can monitor during single measurement. The shorter the distance, the number of measurements increases but also the accuracy of the assessment increases.

The distance between sensors and the size monitored area should be also adjusted not only based on the obtained results and the method accuracy but also on some technical aspects on monitored structure. As mentioned, ships structures are often strengthened by the stiffeners which would be the source of wave reflections affecting the signals and hindering their interpretation. Thus, searching the trade-off between the number of sensors, cost, time consumption, resolution and the accuracy of the method with taking into account the geometry of the monitored structure is one of the essential step towards developing new corrosion assessment procedure.

The results proved that Bilateral and Rotational Corrosion Symmetry Degree (BCSD and RCSD) functions consistently decrease with increasing DoD, indicating the influence of corrosion degradation on wavefront symmetry. The decreasing trend was observed for variable distance between the transducers and for variable extent of the sensor network. However, the more extensive sensor network monitoring was assessed as more efficient due to more significant changes in symmetry degrees. In the case of the smaller number of transducers (4 or 8) in some cases, the decrease of investigated indicators was comparable to measurement error, which is one of the presented approach's drawbacks. Moreover, the number of sensors significantly impacts corrosion monitoring efficiency more than the spatial separation between the actuator and sensors. The size of the monitored area can be adjusted based on the investigator's needs, but the number of sensors remains crucial in wavefront asymmetry analysis. This finding implies the need of the further investigations. The possible solution allowing for reduction of the network extent would be developing the combined algorithms based on e.g., initial scanning the surface by wavefront symmetry assessment and next by more detailed inspection of selected areas with the lowest symmetry levels. The another approach would involve different algorithms of corrosion level assessment i.e. double-step inspection. Estimation of the average thickness based on the averaged wave propagation velocity and next the symmetry assessment would be the additional tool for roughness estimation. Another solution is enriching the algorithms by using additional tools such as neural networks [35,36] which have been proven to be a powerful tool that well expresses the mapping relationship between the inputs and outputs of a structure. However, this needs the further tests and considerations.

The traducers' circular array allowed for monitoring the corrosion process without knowledge of the material parameters of the plate and the dispersion curves usually traced for intact structure. It should be noted here that the algorithm was formulated to exclude the necessity of collecting this data because the reconstructed wavefront was always "normalized" according to the minimal time of flight registered by one of the sensors. Consequently, the length of one of the arms was equal to the distance between the actuator and the sensor. This formulation excluded the need to collect the reference data i.e., material parameters of the tested specimen, which in so far developed methods incorporating dispersion curves was crucial. The main advantage of such modification is less sensitivity to errors in ToF estimation. Wavefront reconstruction does not demand the analysis of the exact value of the ToF but the differences in the ToF measured by different sensors. Therefore, we can avoid the discrepancies in ToF determination caused, e.g., by choosing

different methods of the ToF estimation or due to different initial delays of various devices used in the investigation.

On the other hand, it should be considered that the differences in the ToF may also arise from the inaccurate transducer's attachment. In the case of the relatively low DoD, the asymmetry caused by the specimen degradation may be less noticeable than the asymmetry caused by imperfect experimental conditions. Thus, the next stage of the investigation should focus on the accuracy assessment of the method and on determining the so-called curves presenting the probability of detection for corrosion degradation.

The next limitation of the method is its lack of sensitivity to uniform thickness reduction. As mentioned, the algorithm uses only the differences in the ToF, not the exact values. In the case of the two plates totally differing in thickness but with smooth surfaces, we obtain the exact shape of the propagating wavefront. The solution for this limitation would be enriching the algorithm with an additional part regarding determining the average thickness based on the average wave velocity in a given section. The potential enriching the algorithm with additional determinations of average thickness based on curves would increase the method accuracy but it entail the need of collecting the reference data. In such a case, the method presented in the paper would be used for roughness assessment. In contrast, the so-far-developed algorithms aimed on solving the inverse problem (determining the thickness based on velocity using known shape of the dispersion curves) would be used for the average thickness assessment. The further investigations should also take into account the complex geometry of the tested structure which was omitted in this study. Due to economic aspects, the ship hulls are usually built of sheets varying in thickness. The standard ultrasonic scanning is insensitive to such variability – the results obtained can be easily compared with documentation. However, in the case of guided wave propagation depending on the thickness, the velocity may be anisotropic and the wavefront becomes asymmetric, even for undamaged structure. This anisotropy should be included in the developed algorithm to avoid the misinterpretation of the asymmetric results.

The another source of the potential problems with signals interpretation is the presence of localized damages i.e. pits or cracks. They would be the cause of additional reflections in signals, or in extreme case when located between actuator and sensor could prevent incident wave registration. Despite that the localized damages might be the source of the similar effects to e.g. mentioned above stiffeners, their presence is usually difficult to predict.

Despite mentioned limitations, the obtained results proved that guided waves can be potentially useful for corrosion degradation assessment. The significant influence on the shape of the propagating wavefront had the roughness of the surface, which was clearly visible when wavefront symmetry was analyzed. Even though the whole plate surface has been defined by using a random field with a priori assumed statistical parameters (average thickness and standard deviation), the velocity measured in different directions differed. Future studies should be focused on the inverse problem, i.e., how to obtain the statistical parameters of the surface based on guided wave propagation measurement.

Ethical statement:

The authors state that the research was conducted according to ethical standards.

CRediT authorship contribution statement

Beata Zima: Writing – original draft, Visualization, Supervision, Software, Resources, Project administration, Methodology, Investigation, Funding acquisition, Formal analysis, Conceptualization. **Emil Roch:** Software, Conceptualization.

Declaration of competing interest

The authors declare that they have no known competing financial interests or personal relationships that could have appeared to influence the work reported in this paper.

Data availability

Data will be made available on request.

Acknowledgment

The research was carried out within project No. 2021/43/D/ST8/00786, financed by the National Science Centre, Poland. Abaqus calculations were carried out at the Academic Computer Centre in Gdańsk.

References

[1] F. Qiu, H. Wang, H. Qian, H. Hu, X. Jin, F. Fan, Evaluation of compressive properties of the ship plate after seawater corrosion based on 3D evolution prediction, Ocean Eng. 266 (2022) 112561.
[2] S. Mahadevan, P. Shi, Corrosion fatigue reliability of aging aircraft structures, Prog. Struct. Eng. Mater. 3 (2) (2001) 188–197.
[3] J. Bhandari, F. Khan, R. Abbassi, V. Garaniya, R. Ojeda, Modelling of pitting corrosion in marine and offshore steel structures – A technical review, J. Loss Prev. Process Ind. 37 (2015) 39–62.
[4] International Association of Classification Societies Recommendation 87. Guidelines for Coating Maintenance & Repairs for Ballast Tanks and Combined Cargo/ballast Tanks on Oil Tankers (2015).
[5] K. H. Seah, M. F. Karim, L. C. Ong, and T. M. Chiam, "Rapid corrosion detection using 94 GHz millimeter wave technology," *2012 IEEE International Instrumentation and Measurement Technology Conference Proceedings*, Graz, Austria, 2012, pp. 473-476, doi: 10.1109/I2MTC.2012.6229447.
[6] A. Eddazi, S. Belattar, Nondestructive Testing Evaluation of Aircraft Fuselage Corrosion by Infrared Thermography and Finite Element Method, International Conference on Computer Graphics Imaging and Visualization. (2017) 56–61.
[7] Z. Su, L. Ye, Y. Lu, Guided Lamb waves for identification of damage in composites: A review, J. Sound Vib. 295 (2006) 753–780.
[8] J. Jingpin, M. Xiangji, H. Cunfu, W. Bin, Nonlinear Lamb wave-mixing technique for micro-crack detection in plates, NDT and E Int. 85 (2017) 63–71.
[9] H. Zou, Z. Yang, C. Xu, S. Tian, X. Chen, Damage identification for plate-like structures using ultrasonic guided wave based on improved MUSIC method, Compos. Struct. 203 (2018) 164–171.
[10] Z. Tian, W. Xiao, Z. Ma, L. Yu, Dispersion curve regression – assisted wideband local wavenumber analysis for characterising three-dimensional (3D) profile of hidden corrosion damage, Mech Syst Signal Pr 150 (2021) 107347.
[11] J. Hua, X. Cao, Y. Yi, J. Lin, Time-frequency damage index of Broadband Lamb wave for corrosion inspection, J Sound Vib 464 (2020) 114985.
[12] B. Zima, R. Kedra, Debonding Size Estimation in Reinforced Concrete Beams Using Guided Wave-Based Method, Sensors 20 (2) (2020) 389.
[13] F. Nicassio, S. Carrino, G. Scarselli, Elastic waves interference for the analysis of disbands in single lap joints, Mech. Syst. Signal Process. 128 (2019) 340–351.
[14] A. Farhidzadeh, S. Salamone, Reference-free corrosion damage diagnosis in steel strands using guided ultrasonic waves, Ultrasonics 57 (2015) 198–208.
[15] B. Zima, K. Woloszyk, Y. Garbatov, Experimental and numerical identification of corrosion degradation of aging structural components, Ocean Eng. 258 (2022) 111739.
[16] H. Sun, W. Shao, J. Song, X. Yang, Y. Wang, X. Qing, Corrosion quantification of plate-type structures using Lamb wavefield and monogenic signal processing, Ultrasonics 130 (2023) 106935.
[17] X. Ding, C. Xu, M. Deng, Y. Zhao, X. Bi, N. Hu, Experimental investigation of the surface corrosion damage in plates based on nonlinear Lamb wave methods, NDT&E Int. 121 (2021) 102466.
[18] C. Nicard, M. Farin, E. Moulin, D. Balloy, I. Serre, Monitoring of generalized corrosion: Ultrasonic coda wave interferometry technique applied to steel corrosion in aqueous NaCl solutions, Mater. Chem. Phys. 305 (2023) 127908.
[19] V. Rathod, D. Roy Mahapatra, Ultrasonic lamb wave based monitoring of corrosion type of damage in the plate using a circular array of piezoelectric transducers, NDT&E Int. 44 (2011) 628–636.
[20] B. Zima, E. Roch, J. Moll, Nondestructive corrosion degradation assessment based on asymmetry of guided wave propagation field, Ultrasonics 107243 (2024).
[21] B. Zima, J. Moll, Numerical and experimental investigation of guided ultrasonic wave propagation in non-uniform plates with structural phase variations, Ultrasonics 128 (2023) 106885, https://doi.org/10.1016/j.ultras.2022.106885.
[22] B. Zima, J. Moll, Theoretical and experimental analysis of guided wave propagation in plate-like structures with sinusoidal thickness variations, Arch. Civil and Mech. Eng. 23 (2023) 34, https://doi.org/10.1007/s43452-022-00564-9.
[23] Y. Cho, Estimation of ultrasonic guided wave mode conversion in a plate with thickness variation, IEEE T. Ultrason. Fer. 47 (3) (2000) 591.
[24] M.V. Predoi, M.E.C. El-Kettani, Z. Hamitouche, C.C. Petre, Guided waves in plates with linear variation of thickness, J. Acoust. Soc. Am. 123 (5) (2008) 3834.
[25] P. Marical, M.E.C. El-Kettani, M.V. Predoi, Guided waves in elastic plates with Gaussian section variation Experimental and numerical results, Ultrasonics 47 (2007) 1–9.

[26] Z. Hu, Z. An, Y. Kong, G. Lian, X. Wang, The nonlinear S0 Lamb mode in a plate with a linearly-varying thickness, Ultrasonics 94 (2019) 102–108.
[27] J. Moll, T. Wandowski, P. Malinowski, M. Radzienski, S. Opoka, W. Ostachowicz, Experimental analysis and prediction of antisymmetric wave motion in a tapered anisotropic waveguide, J. Acoust. Soc. Am. 138 (2015) 299–306.
[28] Q. Guo, F. Guo, J. Shao, Irregular shape symmetry analysis: Theory and application to quantitative galaxy classification, IEEE Trans. Pattern Anal. Mach. Intell. 32 (10) (2010) 1730–1743.
[29] L.R. Rabiner, B. Gold, Theory and application of digital signal processing, Prentice-Hall, 1975.
[30] E. Vanmarcke, Random Fields. Analysis and Synthesis, World Scientific Publishing Company, Princeton University, USA, 2010.
[31] P. Contantine, Q. Wang, Random field simulation. MATLAB Central File Exchange. Retrieved June 28, 2023, 2023.
[32] S.P. Huang, S.T. Quek, K.k., Phoon Convergence study of the truncated Karhunen-Loeve expansion for simulation of stochastic processes, Int. J. Numer. Methods Eng. 52 (2001) 1029–1043.
[33] H. Gravenkamp, Efficient simulation of elastic guided waves interacting with notches, adhesive joints, delaminations and inclined edges in plate structures, Ultrasonics 82 (2018) 101–113.
[34] B. Zima, J. Moll, Corrosion damage identification based on the symmetry of propagating wavefield measured by a circular array of piezoelectric transducers: theoretical, experimental and numerical studies, Mechanical Systems and Signal Processing 217 (2024) 111538.
[35] L. Niu, Monitoring of a Frame Structure Model for Damage Identification using Artificial Neural Networks, in: B. Wu (Ed.), Proceedings of the 2nd International Conference on Electronic & Mechanical Engineering and Information Technology (Emeit-2012), Atlantis Press, Paris, 2012. doi: 10.2991/emeit.2012.88.
[36] X.-Y. Guo, S.-E. Fang, Structural parameter identification using physics-informed neutral networks, Measurement 220 (2023) 113334.